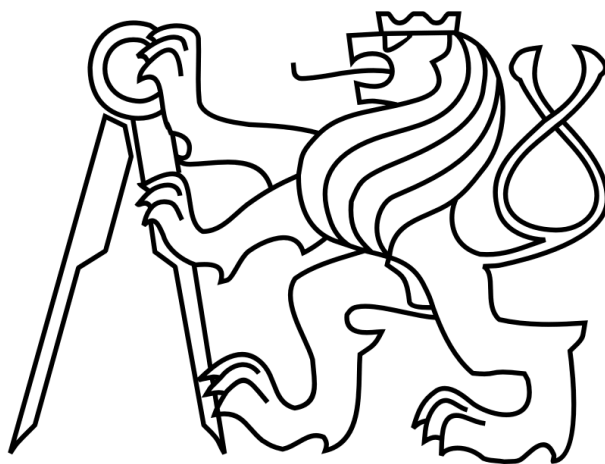


OPTICALLY CONTROLLED AND SENSED MICROMANIPULATION – BASIC SETUP

JAKUB TOMÁŠEK



BACHELOR'S THESIS

Czech Technical University in Prague

Jakub Tomášek: *Optically Controlled and Sensed Micromanipulation – Basic Setup*
BACHELOR'S THESIS

SUPERVISOR:
Ing. Jiří Zemánek

Czech Technical University in Prague
Faculty of Electrical Engineering
Department of Control Engineering

© July 2013

BACHELOR PROJECT ASSIGNMENT

Student: **Jakub Tomášek**

Study programme: Cybernetics and Robotics
Specialisation: Systems and Control

Title of Bachelor Project: **Optically controlled and sensed micromanipulation - basic setup**

Guidelines:

The aim of the project is to design and build a laboratory setup for micromanipulation using an electric field. The position of the object will be sensed through a CCD chip and the electric field will be controlled by light using a spatial light modulator.

1. Design and build a setup for sensing of the object's position through a CCD chip. Consider various kinds of illumination and conduct basic experiments to find out optical performance of the setup.
2. Test and adjust the provided feedback controller for micromanipulation with the translucent electrodes and with sensing by the CCD chip.
3. Design and build a setup for modulating the electric field by incident light. Adapt some suitable design reported in the literature.
4. Create a software for generating image patterns for modulating the electric field. The software will be controlled manually or automatically.
5. Conduct experiments to find out performance of the system for the light modulation and for micromanipulation.

Bibliography/Sources:

- [1] H. Morgan and N. G. Green, AC Electrokinetics: Colloids and Nanoparticles. Research Studies Pr, 2003.
- [2] H. Cho, Optomechatronics: Fusion of Optical and Mechatronic Engineering, 1st ed. CRC Press, 2005.
- [3] T.-M. Yu et al., Organic photoconductive dielectrophoresis by using titanium oxide phthalocyanine for micro-particles manipulation, 2010, pp. 1119-1122.
- [4] P. Y. Chiou, A. T. Ohta, and M. C. Wu, Massively parallel manipulation of single cells and microparticles using optical images, Nature, vol. 436, no. 7049, pp. 370-372, Jul. 2005.

Bachelor Project Supervisor: Ing. Jiří Zemánek

Valid until the winter semester 2013/2014


prof. Ing. Michael Šebek, DrSc.
Head of Department




prof. Ing. Pavel Ripka, CSc.
Dean

Prague, February 11, 2013

ABSTRACT

This thesis investigates two topics related to the use of optics in dielectrophoresis. First, it focuses on optically induced dielectrophoresis, which is a physical phenomenon enabling contactless manipulation with microparticles by projecting specialized light patterns onto a substrate. The main outcomes of the thesis are the design and the realization of a laboratory setup. In addition, numerous experiments were carried out to confirm the functionality. In the experiments, negative dielectrophoretic force induced by the image patterns was observed. Second, the thesis examines the applicability of a cheap lensless CMOS image sensor as a minimalistic solution for an optical feedback for fluidic micromanipulation platforms. The sensor can detect objects as small as $5\text{ }\mu\text{m}$, for example yeast cells. Also, a precise feedback manipulation with 50-micron polystyrene beads is demonstrated. It is shown that the accuracy provided by this cheap lensless sensor is comparable to that provided by a bulky combination of a standard microscope and an off-the-shelf camera. The experiments in both parts of the thesis are accompanied by numerical simulations.

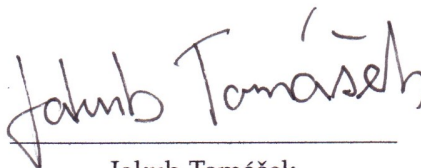
ABSTRAKT

Tato práce zpracovává dvě témata související s využitím optických systémů pro manipulaci pomocí dielektroforézy. V první části se zaměřuje na opticky indukovanou dielektroforézu, která umožňuje manipulaci s mikročásticemi pomocí dynamických světelných obrazců. Zde je hlavním výstupem navržení a postavení laboratorní sestavy, na které byly testovány různé zobrazovací metody a fotosenzitivní materiály. V experimentech byla pozorována negativní dielektroforetická síla. V druhé pasáži je pak zkoumána využitelnost obrazového senzoru bez optiky v platformách pro automatickou mikromanipulaci v kapalinách. Levný CMOS senzor umožnil detekci objektů s rozměry od $5\text{ }\mu\text{m}$ – například kvasinek. S použitím tohoto levného senzoru je nakonec demonstrována přesná zpětnovazební manipulaci s polystyrenovými mikrokuličkami. Ukázalo se, že v takovém úkolu senzor nabízí podobnou přesnost jako drahá a objemná kombinace standardního mikroskopu a kamery. Experimenty jsou v obou částech práce podpořeny numerickými simulacemi.

DECLARATION

I hereby declare that this thesis is my own work and effort. Where other sources of information have been used, they have been acknowledged.

Prague, July 2013

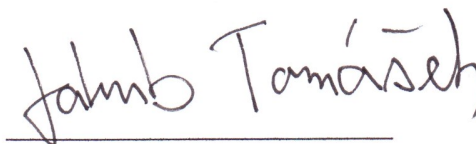


Jakub Tomášek

PROHLÁŠENÍ

Prohlašuji, že jsem předloženou práci vypracoval samostatně a uvedl veškeré použité informační zdroje v souladu s Metodickým pokynem o dodržování etických principů při přípravě vysokoškolských závěrečných prací.

Praha, červenec 2013



Jakub Tomášek

ACKNOWLEDGMENTS

Above all, I owe my deepest gratitude to my supervisor, Mr. Jiří Zemánek, for his guidance, patience, and caring manner. He has never refused to offer an advice or help.

Special thanks also to Dr. Zdeněk Hurák for priceless advices, inspiration and mentoring.

I appreciate the insightful feedback offered by Jindřich Prokop, Martin Gurtner and Jiří Figura. All these people made the past year at Department of Control Engineering more enjoyable.

Finally, I would like to thank to Bérénice Verdier and Linda Ševčíková for their countless language advices. They made this thesis readable.

CONTENTS

1	INTRODUCTION	1
1.1	Motivation	1
1.2	DEP manipulation based on microelectrode arrays	1
1.3	Optically induced dielectrophoresis	3
1.4	Means of optical feedback: the lensless sensor	3
1.5	Thesis structure	4
2	OPTICALLY INDUCED DIELECTROPHORESIS	5
2.1	General principle of oiDEP	5
2.2	Dielectrophoresis	5
2.3	Electroosmosis	8
2.4	Recent development in oiDEP	9
2.5	OiDEP chip: design and fabrication	11
2.6	Model and simulations	13
3	OPTICAL FEEDBACK: USING A LENSLESS SENSOR	23
3.1	Image sensors	23
3.2	Experiments and discussion	24
3.3	Light absorption and scattering by small particles	26
4	DEVICE FOR AUTOMATIC MICROMANIPULATION BASED ON OI DEP	31
4.1	General setup	31
4.2	Optical system	31
4.3	Software	35
4.4	Laboratory setup	36
4.5	Experiments and discussion	38
5	TRANSLUCENT ELECTRODE ARRAY WITH VISUAL FEEDBACK	43
5.1	Translucent microelectrode array: its fabrication and design	43
5.2	Experimental setup	44
5.3	CMOS sensor	44
5.4	Control law	47
5.5	Results and discussion	48
5.6	Conclusion	51
6	SUMMARY AND FUTURE WORK	53
6.1	Optically induced dielectrophoresis	53
6.2	Lensless sensor	53
I	APPENDIX	55
A	SOFTWARE	57
A.1	Software for automatic control	57
A.2	Software for manual control	61

B	INDEPENDENT CONTROL OF MULTIPLE OBJECTS ON AN INTERDIGITATED ARRAY	63
B.1	The algorithm for object interchanging	63
B.2	Experiments and discussion	63
C	CD CONTENTS	67
	BIBLIOGRAPHY	69

ACRONYMS

a-Si:H	hydrogenated amorphous silicon
AA4CC	Advanced Algorithms for Control and Communications research group
CdS	cadmium sulfide
DCE	Department of Control Engineering
DEP	dielectrophoresis
DLP	Digital Light Processing
DVS	Dynamic Vision Sensor
FEM	finite element method
GUI	graphical user interface
ITO	indium tin oxide
LC	liquid crystal
LCoS	liquid crystal on silicon
LiF	lithium fluoride
LRA*	local repair A*
MEA	micro-electrode array
nDEP	negative dielectrophoresis
OET	optoelectric tweezers
oiDEP	optically-induced dielectrophoresis
OpenCV	Open Source Computer Vision
P ₃ HT:PCBM	Poly-3-hexyl thiophene:Phenyl-C ₆₁ -butyric acid methyl ester
PCB	printed circuit board
pDEP	positive dielectrophoresis
PDMS	Polydimethylsiloxane
PEDOT:PSS	poly(3,4-ethylenedioxythiophene) poly(styrenesulfonate)

PMMA	poly(methyl methacrylate)
PS	polystyrene
TiOPc	titanyl phthalocyanine
WHCA*	windowed hierarchical cooperative A*

INTRODUCTION

1.1 MOTIVATION

Recent efforts and achievements in fluidic microassembly and micro-manipulation are gaining more attention from the experts in biomedicine, chemistry and microelectronics, among others. In this matter, dielectrophoresis (DEP) has emerged as one of the methods available for micromanipulation; it fills the niche among technologies such as optical tweezers, acoustic waves or mechanical manipulators. It has been receiving serious research attention in the course of last twenty years [28].

There is a number of reasons for the growing interest in DEP. DEP induces motion of electrically-neutral particle through the interaction of a non-uniform electric field and an induced electric dipole. In comparison with the rival technologies, DEP offers several advantages like contactless and massively parallel manipulation, attractive and repulsive forces, low field energies, and no need for labelling. Above all, the cutting edge of DEP is in its simplicity.

In the future, DEP could have an essential role in a wide spectrum of disciplines. It has turned out to be a promising tool for a selective manipulation and separation of cells. Namely, detachment of leukaemia and breast-cancer cells from blood [17], dead from living cells [31], viable from unviable yeast cells [24] were demonstrated, to mention a few. Also DNA, proteins and stem cells seem to be receptive to the dielectrophoretic force [28]. There, DEP could be an important stepping stone in these currently growing fields. Further, DEP could be feasible in the assembly of nanotubes, nanowires or sensors [13].

Despite all that, automation hasn't yet fully penetrated into the field of DEP. There has been only a partial endeavour to demonstrate automated manipulation using DEP [7, 16, 26]. There are many challenges yet to be solved in this field.

1.2 DEP MANIPULATION BASED ON MICROELECTRODE ARRAYS

As a part of the research of distributed planar manipulation at Advanced Algorithms for Control and Communications research group (AA4CC) at Department of Control Engineering (DCE) there has been done extensive work regarding the technology of DEP [43, 44, 41].

By applying different electric signal on microelectrodes distributed in a special layout in a plane we achieve the inhomogeneity of the electric field which is necessary to induce the DEP force. The electrodes

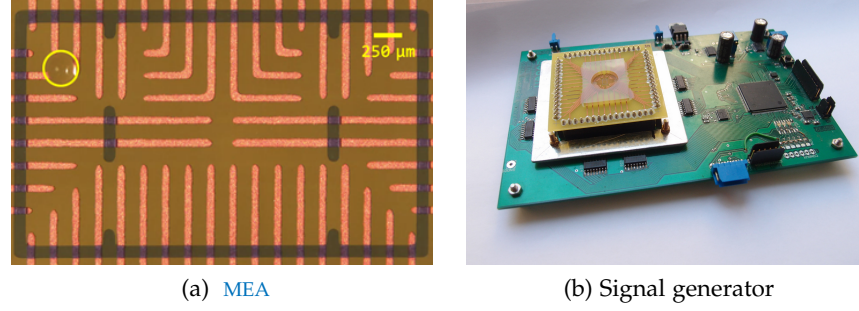


Figure 1: Example of the micromanipulation with DEP by employing the MEA. The image in (a) was captured using camera with $4\times$ Olympus lenses. It shows a detail of MEA with a 250-micron PS bead and the arena. Electrodes are reddish and the bead is highlighted. The array is connected with the 64-channel signal generator in (b).

form a micro-electrode array (MEA) which is then placed under a liquid with microparticles. A number of different layouts of MEA were designed and fabricated with the purpose to shape an electric field in such way that an object, e.g. a polystyrene (PS) bead or a cell, disposed in a fluid moves in the desired manner. For example see MEA in Figure 1a which was specially designated to steer the particle around along a trajectory in a shape of the number eight. Although originally the MEA was fabricated using a lift-off lithography, we currently employ an easier and cheaper process which uses only ordinary printed circuit board (PCB) techniques. This method of fabrication increases the feasibility of the technology.

On individual electrodes we can change amplitude, phase or shape of the signal to create the non-uniformity of the electric field in the fluid above the MEA. For example, the signal generator displayed in Figure 1b allows us to change the phase of the signal for 64 electrodes separately; it can be controlled from the computer via serial port. Meanwhile, the amplitude and frequency remain identical. The generator has a special interface which enables the connection of all the 64 output channels with the MEA.

The change of phase has proved to be very convenient for the particle control. A PS bead in deionized water is repelled from the electrode with different phase. We used the minimalistic setup depicted in Figure 1 in Microrobotic Challenge at IEEE ICRA in May 2013. The target was to complete a path in a shape of the number eight in the arena with a micro-object in the shortest time possible. The MEA in Figure 1a was specially designed to achieve the trajectory.

There are other devices we have available. For instance, in chapter 5 I use a bipolar signal modulator to change the amplitude of the signal.

1.3 OPTICALLY INDUCED DIELECTROPHORESIS

Fixed electrode array is, however, a limiting factor. For instance, only certain types of movement are possible and thus the array must be designed and manufactured separately for every application. Using the MEA brings additional troubles; generation of the multiple channel high-frequency signal and its connection with the fragile array can be challenging and expensive tasks. Further, it is not easy to find an universal rule for the automatic control of such system. For example, at the moment, we use a simple if-then strategy to control the particle movement.

Therefore, it would be interesting to be able to change the pattern of the electrodes. It is optically-induced dielectrophoresis (oiDEP) which gives us such flexibility.

In oiDEP, we literally draw the electrodes on a chip using a beam of light. As it is described later in chapter 2, there is only one signal applied to two parallel plate electrodes. To enable optical control of DEP in between these electrodes we employ a photoconductive material; i.e. a material which changes its conductivity locally with a change of the incident light intensity. Although we loose the control over the phase and the amplitude of the signal, the proportional control of the induced forces remains through possible variation of the light intensity and wavelength. Hence, it gives us an extra degree of freedom and changes the approach towards the manipulation in comparison with the MEA. Much simpler path can be taken to control particles only locally. When sufficient spatial resolution of the light projection is achieved we can even address every object separately.

In this thesis, the oiDEP is used as the core element of the optically controlled platform.

1.4 MEANS OF OPTICAL FEEDBACK: THE LENSLESS SENSOR

Presently, in our laboratory, a microscope is used as a means of optical feedback for the automated manipulation. It is a common practice in this field. However, the specific scale of the micromanipulation, i.e. the size of the objects and the area, is comparable with dimensions of contemporary image sensors that are used in cameras. We target to manipulate objects with size from 5 μm to 250 μm over distances in the order of millimetres. Meanwhile the size of the image sensors used in ordinary cameras ranges from 1 mm up to 55 mm. That is very convenient. We could try cutting the lens out of the loop and place the liquid with particles directly above the image sensor.

Thanks to the popularity of cameras and camera smartphones, factories produce the image sensors in huge bulks every day. Thus the price of the sensor in the microscope is negligible in comparison with the rest, i.e. the optics and the microscope frame. Moreover the mi-

croscope is a bulky device. All that is a strong restriction for the wider expansions of micromanipulation technology beyond the door of chemical and biological laboratories where the microscopes are easily accessible. The replacement of the bulky microscope with a tiny lensless sensor seems to be a great improvement which is even more highlighting the minimalistic properties of the DEP technology.

The lensless sensor technology is not bounded with oiDEP but it could an extremely beneficial combination for various reasons. The lensless sensor can be also used as a feedback for MEA-based DEP manipulation. Only, we need to fabricate the electrodes with a translucent material, for example indium tin oxide (ITO), on a transparent sheet, e.g. on a sheet of glass.

1.5 THESIS STRUCTURE

In my thesis, I adapted the basic ideas described above. Based on these ideas, state-of-the-art research publications, and the know-how at the AA4CC in the field of DEP I designed and built a laboratory setup for oiDEP micromanipulation. Also, we started a cooperation with Polymer Photonics Department at the Institute of Macromolecular Chemistry of the ASCR. They provided me unique polymer materials necessary for the oiDEP device fabrication.

oiDEP is thoroughly examined in chapter 2. I performed various simulations using finite element method (FEM) software to have the initial estimates of the performance and the necessary dimensions.

Chapter 4 is almost all designated for the experiments. There, I describe the oiDEP device and discuss the laboratory setup. I was able to verify that the concept works although I didn't demonstrate full manipulation.

Besides that, I review the use of the lensless sensor for micromanipulation in the separate chapters 3 and 5. In the latter, I used a translucent interdigitated MEA combined with a lensless-sensor for feedback manipulation. In the experiments I demonstrated that with the cheap lensless sensor it is possible to achieve the level of precision in position as good as with the microscope camera.

Finally, in the appendix, I include a detailed description of the software I created for the platform. Additionally, there I show that it is feasible to control multiple objects on a simple interdigitated array.

OPTICALLY INDUCED DIELECTROPHORESIS

2.1 GENERAL PRINCIPLE OF OIDEP

The idea behind **oiDEP** is to use a difference between the electrical properties at lit and unlit areas of a photosensitive layer to modulate an electric field. A layout described below in [section 2.5](#) creates such non-uniformity of the electric field that the induced **DEP** force either repels objects from or attracts them towards the edges of the illumination. In consequence, the light creates virtual electrodes with properties similar to the fixed electrodes on a **MEA** introduced in [section 1.2](#). [Figure 2](#) which illustrates the difference between these two approaches.

2.2 DIELECTROPHORESIS

The term *dielectrophoresis* suggests its relation to the more known effect - *electrophoresis*. *Electrophoresis* describes the movement of charged particles through a solution under the influence of an applied electric field. Meanwhile, Pohl [30] defined **DEP** as “the motion of suspensoid particles relative to that of the solvent resulting from polarization forces produced by an inhomogeneous electric field”. While *electrophoresis* is simply represented by Coulomb force, the model of **DEP** is significantly more complicated.

DEP force emerges from the accumulation of charge on the interface of two dielectrics with different electrical properties, i.e. permittivity and conductivity, in an electric field. An example of the two dielectrics could be a pair of a spherical particle and a fluid.

A sphere immersed in a liquid and placed in an electric field is the case typically modelled in literature as it is relevant to the real world. The charge accumulation around the sphere can be visualized

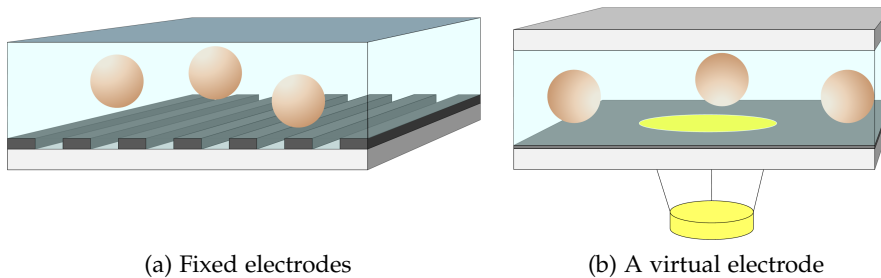


Figure 2: Fixed electrodes (a) in comparison with the virtual electrodes (b).

as a multipole. Thus the electrically neutral particle does not move when the field is uniform. The problem is further simplified; dipole description is a generally accepted model for this situation.

DEP propelling of the spherical particle is generally modelled as the electric force, which acts on the induced dipole. The time-averaged DEP force is:

$$\langle \mathbf{F}_{\text{DEP}} \rangle = \pi \epsilon_m r^3 \Re [\tilde{f}_{CM}] \nabla |\mathbf{E}|^2, \quad (1)$$

$$\tilde{f}_{CM} = \frac{\tilde{\epsilon}_p - \tilde{\epsilon}_m}{\tilde{\epsilon}_p + 2\tilde{\epsilon}_m}, \quad (2)$$

DEP force is
frequency dependent.
Its direction
correlates with the
electric field
magnitude gradient.

where $\langle \mathbf{F}_{\text{DEP}} \rangle$ is the vector of the time averaged DEP force¹, \mathbf{E} is the vector of the electric field while $|\mathbf{E}|$ is its magnitude, \tilde{f}_{CM} is the Clausius-Mossoti factor², r is the radius of the sphere, ϵ is the permittivity and $\tilde{\epsilon}$ is the complex permittivity. Indexes p and m refer to *particle* and *medium* respectively in the whole thesis.

Several assumptions are made to obtain this simplified model:

- the phase of the electric field is constant,
- the particle diameter is smaller than a typical non-uniformity of the field,
- the particle is ideal homogeneous sphere.

The latter can be problematic if we wished to consider for example manipulation with cells. In that case, it would be better to enhance the model by using induced dipole adapted for a shell sphere. That leads to a modification of the Clausius-Mossoti factor. Pethig [29] suggests to refine the model by incorporation of the multipole theory. Additionally, there are other effects such as a double layer which could be relevant in some models.

In my experiments I used spherical PS beads with diameter ranging from 5 μm to 250 μm and invariable phase of the electric field. Therefore, this model should be sufficient for our requirements.

There is a number of consequences of the (1). The most important is the dependence of the DEP force on the gradient of the square amplitude of the electric field intensity. It determines the direction of the force.

2.2.2.1 Clausius-Mossoti factor

The direction of the force is secondly characterized by the real value of the \tilde{f}_{CM} and thus, according to (2), by complex permittivities $\tilde{\epsilon}$ of

¹ The derivation of (1) is interesting but not trivial and important for understanding of the following text. Thus I haven't included it in this work but one can find very illustrative derivation for example in [25] or in [29].

² \sim denotes complex number.

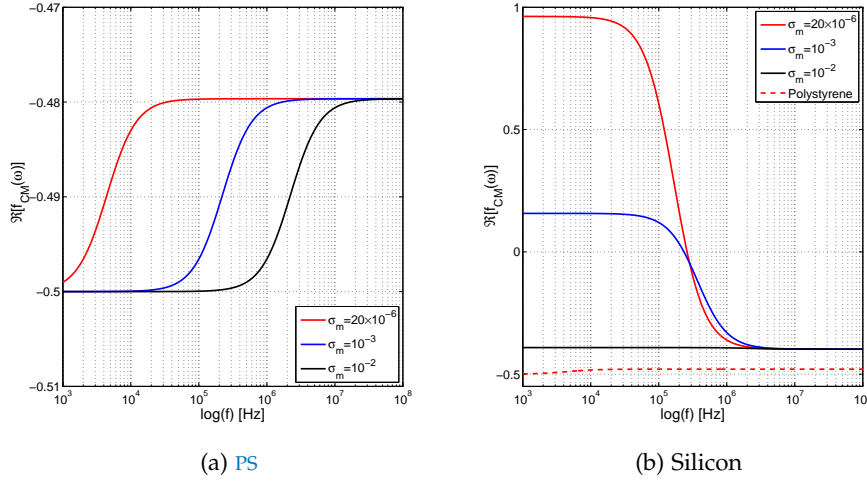


Figure 3: Real part of Clausius-Mossotti factor as a function of frequency. Solution for (a) PS and (b) silica particles in deionized water ($\epsilon_r = 80$) and water with varying conductivity σ_m . In (b), there is additionally plotted PS dependence for comparison.

the particle and the medium:

$$\tilde{\epsilon}_x = \epsilon_x - j \frac{\sigma_x}{\omega}. \quad (3)$$

σ_x is the conductivity of either the medium or the sphere. Complex permittivity expresses properties of a lossy dielectric in an electric field. Hence, \tilde{f}_{CM} is a complex and frequency dependent parameter; it describes a relaxation in the effective permittivity or polarizability of the particle. The real value of Equation 2 ranges from $\frac{\sigma_p - \sigma_m}{\sigma_p + 2\sigma_m}$ for the low frequency to $\frac{\epsilon_p - \epsilon_m}{\epsilon_p + 2\epsilon_m}$ for the high frequency [25]. Thus the factor can be either *positive* or *negative*. We refer to this as positive dielectrophoresis (pDEP) and negative dielectrophoresis (nDEP) respectively. In the first case, the particle moves towards the area of stronger electric field, whereas, nDEP drives the particles in the opposite direction to the weaker electric field region. The effect could enable us to attract and repel particles by a simple change of frequency and it can be classified among number of DEP advantages.

In (1) Clausius-Mossotti factor represents the properties of the dielectric interface between the particle and the medium. It is obvious that electrical properties of the particle determine the value of the factor. Thus the DEP force differs with the type of the particle. It is possible to achieve such arrangement that while the factor is positive for one type of particles, it is negative for the other. Hence the possibility of cell separation emerges [31, 17]. Moreover, in manipulation the phenomenon might allow us to address only one type of particles by the frequency change.

Figure 3 demonstrates values of the Clausius-Mossotti factor as a function of frequency for PS and silica particles immersed in water with variable conductivity. That simulates how the factor changes when we add ions in the deionized water, e.g. dissolve salt. In my experiments, however, I used only deionized water with electrical conductivity varying from $17 \mu\text{S m}^{-1}$ up to $50 \mu\text{S m}^{-1}$ and PS beads with low conductivity around $1 \times 10^{-16} \text{ S m}^{-1}$. It is clear from the Figure 3 that only nDEP force can be attained with this material combination. It is convenient that frequency change of the factor is minimal and thus slightly different conductivity of water should not have a significant effect on our experiments.

2.3 ELECTROOSMOSIS

Additional effect occurs in the liquids placed in electric fields. Electroosmosis causes a flow of the medium; due to the viscous drag, all the objects in the medium are propelled along with the fluid in motion. In itself, the electroosmosis is an extremely useful effect in many applications. For instance, it is often used in capillaries to sort and transport nanoscale particles [12], or for pumping fluid through microchannels [10]. However, in DEP manipulation it is considered rather negatively [32].

Electroosmosis describes the flow in a medium caused by charges moving due to the applied electric field.

Its origin is in the Coulomb force. Upon an electrode with a positive or negative potential immersed in a liquid, e.g. water, a thin layer of free charges with opposite charge, like ions, is formed. It is called *double layer* due to its structure. Tangential electric field causes the movement of the charge along the electrode. The charges pull the fluid along due to the viscous drag; that induces the medium movement in the vicinity along the surface of the electrode.

The behaviour was originally described for the DC electric field. Yet, literature reported frequency dependent fluid motion for the alternating field caused by electroosmosis [11, 32]. It is now well established as AC electroosmosis. However, only a non-uniform electric field can induce the flow since a component of the field must be tangential to the electrode.

There are four major factors that determine the magnitude of the electroosmosis:

1. frequency and amplitude of the applied AC field,
2. viscosity of the medium,
3. conductivity of the medium,
4. the scale of the system.

The force is stronger at lower frequency region as there is enough time for the double layer to form. In addition, it is obvious that this

effect is more pronounced in the fluids with higher conductivity³. Nevertheless, I witnessed the effect even in deionized water used in our experiments. The effect was observable in frequencies below approximately 100 kHz. That agrees with the theory [25].

2.4 RECENT DEVELOPMENT IN OIDEF

This section briefly reviews the current state of the art in *oiDEP* with few highlighted publications from the preceding years. I tried to concisely compare the different approaches to the problem such as the material and employed projection methods.

The seminal paper [5] was published almost 10 years ago. In the paper, Chiou pioneered the *oiDEP* manipulation using a 633-nm laser with intensity slightly more than 0.2 W cm^{-2} and 2-microns-thick photoconductive layer of hydrogenated amorphous silicon (a-Si:H). There, latex particles with diameter $25 \mu\text{m}$ were moved with maximum speed $397 \mu\text{m s}^{-1}$ when 10 V AC voltage was applied.

Chiou uses an alternative title optoelectric tweezers (OET); it is supposed to induce the part resemblance with the optical tweezers which, however, are based on a diametrically different principle⁴. Not all laboratories followed Chiou in the terminology and thus even I am trying to avoid the term as it brings natural confusion for the reader not familiar with the field.

Later, Chiou describes the *oiDEP* concept in depth in a dissertation [4]. Most importantly, he demonstrates that it is possible to move the particles using only a conventional light source, for example a Digital Light Processing (DLP) projector. I based my work greatly upon this dissertation.

Only recently, *oiDEP* has drawn serious attention of other laboratories around the world. Chiou's group has refined the technology for example by adding other layers in the *oiDEP* chip in order to avoid direct contact of the photoconductive material with the liquid and and electrolysis. Later they tried to replace the photoconductive material with phototransistors [15]. Further, a manipulation with various cell types [6, 26, 19, 9] or an assembly of metallic nanowires [20] were demonstrated. Also different display techniques were reported to be feasible, for example LCD in [19].

³ Higher conductivity of the medium is typical for cell manipulation. The cell solution must be often iso-osmotic so the cells will not be damaged [25]. Conductivity of stationary human blood at 37°C ranges from 0.15 S m^{-1} to 1.55 S m^{-1} [37]. Meanwhile conductivity of deionized water is around $20 \mu\text{S m}^{-1}$.

⁴ Optical tweezers use a high power beam of laser focused in a small area to create optical traps with very strong electric field gradient. Unlike the *oiDEP*, it uses direct optical forces for the particle manipulation. The disadvantages are the high optical power (according to [4], minimal power is $1 \text{ mW } \mu\text{m}^{-2}$), only small reach and the high cost. In *oiDEP*, optical energy is converted to the mechanical energy in an indirect way.

material	v [$\frac{\mu\text{m}}{\text{s}}$]	F [pN]	particles	medium	source	I [$\frac{\text{mW}}{\text{cm}^2}$]	V_{pp} [V]	f [kHz]	
a-Si:H	397	-	20 μm , PS	0.01 S m ⁻¹	laser	1000	10	100	[4]
P ₃ HT:PCBM	202.2	38.2	20 μm , PS	water	mercury	7800	24	100	[38]
CdS	-	6	10 μm , PMMA	water	xenon	14.4	~ 10	$\times 0.01$	[14]
TiOPc	10	40	16 μm	water	-	-	10	1	[40]
TiOPc	160	50	300 pl, gas	silicone oil	mercury	0.33	10	100	[39]

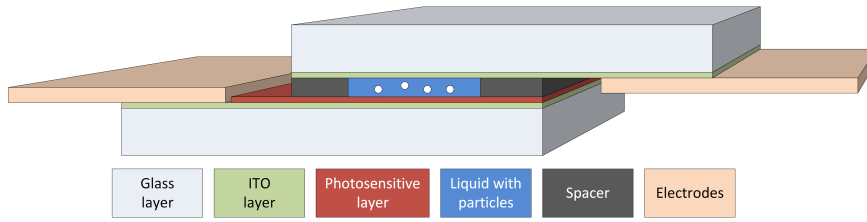
Table 1: A comparison of the performance for different photoconductive materials reported in literature. The conditions of the experiments substantially differed; thus, the results are only indicative. v and F are the velocity and the force observed in the listed publications, I is the intensity of the used light source. xenon and mercury refer to a xenon arc lamp and a mercury lamp respectively. Those light sources were built in a projector.

2.4.1 Photoconductive layer

It turns out that the used material for the photoconductive layer has an essential role for the properties of the whole device. For example it determines the type of the light source used.

In the past decade, a host of distinct materials for the photoconductive layer has been tested apart from the original a-Si:H. Most of these materials has been already used in different fields such as laser printers or solar cells, however, their purpose is very similar in these applications.

For instance, in [14] poly(methyl methacrylate) (PMMA) particles are moved using a cadmium sulfide (CdS) substrate. Conveniently, CdS absorbs only in the blue light region. Meanwhile red light is transmitted and thus it can be used for the observation. Further, [38] uses polymer Poly-3-hexyl thiophene:Phenyl-C₆₁-butyric acid methyl ester (P₃HT:PCBM) in the photoconductive layer. The setup induced maximum force 38.2 pN. The force on 20- μm PS beads moved particles with maximum speed 202.2 $\mu\text{m s}^{-1}$ when the P₃HT:PCBM layer was 500 nm thick. However, the lifetime of this chip version was very limited (only around 5 hours). Finally, organic substrates performed very well in this task. In [40, 39], they utilized titanyl phthalocyanine (TiOPc). With intensity of the light only around 0.3 mW cm⁻² they report force around 160 pN. All the materials are summarized and compared in Table 1; the table also lists other conditions of the experiment like the applied voltage, used objects, or type of the light source and its intensity.

Figure 4: *oi*DEF chip structure

2.5 OIDEF CHIP: DESIGN AND FABRICATION

The analysis of the problem results in a slightly different realization of the *oi*DEF device when compared with MEA. Its layout is illustrated in Figure 4⁵. The *oi*DEF chip, which carries the liquid with the particles, is the core of the whole device.

To build the *oi*DEF chip, firstly, we sandwich the liquid with microparticles in between two glass sheets coated with a transparent conductive layer. For example, heavily doped ITO is a suitable and widely used material for that purpose. The glass sheets coated with ITO are easily available on the European market since they are extensively used in other popular applications such as photovoltaic cells and LCD technology. The layers serve as planar electrodes; they are directly connected to some signal generator. A spacer provides certain distance between the electrodes. We obtain a device similar to the plate capacitor.

The crucial part of the *oi*DEF chip is the photoconductive layer coated upon one of the electrodes. Excitation of electron-hole pairs by electromagnetic radiation in the lit area causes few order decrease in the impedance. Hence, the voltage across the fluid leaps and the electric field distribution changes. That finally causes a non-uniformity of the electric field and induces the DEF force (1). Particles immersed in the fluid placed upon these electrodes should be either repelled away or attracted towards them. This allows us to move objects and control their position with a beam of light.

The chip is placed in a horizontal position and the light can be projected on the chip from top or bottom.

To achieve sufficient inhomogeneity of the electric field the virtual electrodes created by light must be sharp-edged. This rises specific requirements on the photoconductive material; it is essential that the produced electron-hole pairs in the material have a short diffusion length [8]. The diffusion length of the material is determined by the mobility and recombination time of the electric charge carriers. That limits the spectrum of usable materials.

The design is very similar to the design of a parallel plate capacitor. Additional layer of photosensitive material allows us to modulate the electric field inside and achieve the non-uniform electric field.

⁵ I will refer to this layout as the *oi*DEF chip.

2.5.1 Photoconductive layer fabrication

TiOPc

The first material I pursued for the fabrication of the photoconductive layer was TiOPc based on [40]. This organic material is extensively used in new laser printers, in which it is coated upon the drum. TiOPc gives the drums the typical blue colour. It has almost fully replaced the originally employed CdS. It enables a control of the charge spatial distribution upon the drum by a laser beam. The material is suitable for high resolution print because the generated electron-hole pair diffusion is short. Therefore it is also usable for the oiDEP chip fabrication. Moreover, the application in the laser printers proved the long life-time and durability of the layer.

Other strong advantage of the material is the simple fabrication achievable even in the conditions of our lab. According to [40], the 300-nm-thick layer is spin-coated (1500 rpm, 20 seconds) on the ITO glass sheet. Then, it is baked at 120 °C for 30 min. This method should allow a stable function for more than four months.

Finally, the absorption spectrum of TiOPc peaks around 630 nm. It is beneficial for us since we are already equipped with a laser with wavelength 635 nm.

Nevertheless, we were not able to find a supplier for the material in Europe. The material is available here only in the raw form and we and our partners do not have the necessary know-how to fabricate the solution similar to the one used in the laser printers. This solution is available on the Asian market but it is not easily shippable to Europe.

I tried extracting the material straightly from an old printer toner. At first, I made an attempt to dissolve it using Cyclohexane⁶. The idea was that it would be possible to coat it back on an ITO glass. This way did not seem viable.

Then, I tested whether it wouldn't be possible to build an one-sided oiDEP chip straightly on the drum. After removing the top transport layer we attached an ITO PMMA sheet upon the surface. In between we put particles with liquid. Then we beamed the laser light with wavelength 635 nm and UV LED upon the surface.

Yet these experiments were not successful and I did not observe any movement. It is possible that the failure in the second experiment was caused by the wear of the TiOPc drum. For that, I additionally tried to measure the resistance and its change with incident light in between the ITO sheet and the bottom electrode. Firstly, I measured it in the original composition with water in between. Secondly, the upper electrode was attached straightly to the ITO layer by two-sided transparent conductive tape. However, I didn't make any signific-

⁶ In a commercially available product Čikuli.

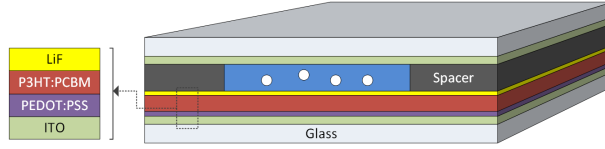


Figure 5: Composition of the photosensitive layer using polymers in detail. A thin layer (30 nm thick) of PEDOT:PSS interfaces the ITO layer and photoconductive P₃HT:PCBM layer (100 nm to 500 nm thick). It decreases the roughness of the ITO layer while it increases the degree of electron injection. Top LiF layer (5 nm thick) protects the P₃HT:PCBM layer from oxidation and the direct contact with the liquid. A similar structure is also typically used in the solar cells.

ant correlation between the amount of light and resistance similar to those when I tested a P₃HT:PCBM layer later.

Therefore I abandoned this solution for the moment. Despite all that, I believe the advantages of TiOPc are worth to return back to it in the future.

Polymer Materials

We initiated a cooperation with the Polymer Photonics Department at the Institute of Macromolecular Chemistry of the ASCR. For the experiments, they provided me with oiDEP-chip samples fabricated according to [38].

In the article, commercially widespread photoconductive polymer P₃HT:PCBM is used. There are two layers in addition to the photoconductive layer. Figure 5 shows the chip structure in detail. A thin layer (30 nm thick) of PEDOT:PSS interfaces the ITO layer and photoconductive P₃HT:PCBM layer (100 nm to 500 nm thick). The PEDOT:PSS layer decreases the roughness of the ITO layer while it increases the degree of electron injection. Top LiF layer (5 nm thick) protects the P₃HT:PCBM layer from oxidation and the direct contact with the liquid. A similar structure is also typically used in the solar cells.

In total, I had 4 samples - X₁ ÷ X₄. Besides the widespread polymer from the article, I could also test a unique polymer with code name K21-2 which was synthesized in the laboratory. It was used in the layers X₃ and X₄ in ratio 1:1 with the P₃HT:PCBM. The spectrum of these two samples peaked approximately at 720 nm but it should be responsive even at lower wavelengths; see Figure 6b. On the other hand, the spectrum of the X₁ and X₂ with pure P₃HT:PCBM layer climaxed around 500 nm.

2.6 MODEL AND SIMULATIONS

In order to explore the properties of the proposed oiDEP chip before fabrication I created a simplified model of the chip. The goal was

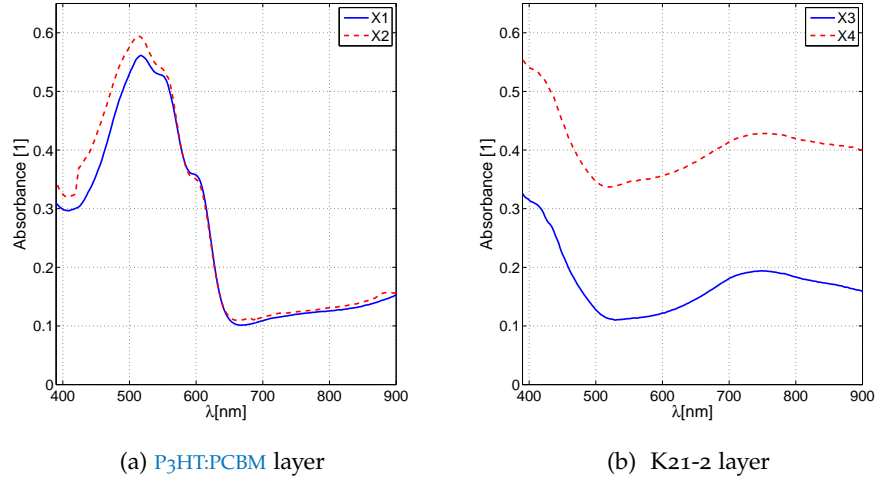


Figure 6: Absorption spectra of the four polymer samples used for the α DEP chip in my experiments. The values in the figures (a) and (b) are not comparable because a correction for the glass sheet was not done properly. The purpose was to determine the peak values to adapt the light source.

to simulate the shape of the field induced when light patterns are incident upon the photoconductive layer. Further, I simulated the trajectory of a particle placed within such field in a liquid.

In the model I incorporated both effects which are described earlier in this chapter:

- DEP force,
- electroosmotic flow.

This problem, of course, leads to the solution of a system of partial differential equations. To find the solution I used FEM⁷. I finally opted for the commercial FEM software Comsol Multiphysics in version 4.3.

2.6.1 Governing equations

This model encompass various physics. The solution to the applied electric field revolves around the continuity equation:

$$\nabla \mathbf{J} = -\frac{\partial \rho}{\partial t}, \quad (4)$$

$$\mathbf{J} = \mathbf{J}_{\text{free}} + \mathbf{J}_{\text{displacement}} = \sigma \mathbf{E} + \frac{\partial \mathbf{D}}{\partial t}, \quad (5)$$

$$\mathbf{E} = -\nabla V. \quad (6)$$

⁷ Although FEM finds only approximate solution it is one of the essential numerical techniques for solving problems with distributed parameters. Yet, there are other methods for solving partial differential equations.

\mathbf{J} is the current density, ρ is the charge density, \mathbf{E} is the electric field, t is the time, V is the potential, and \mathbf{D} is the electric displacement field.

Further, Navier-Stokes equation describes the incompressible flow ($\nabla \cdot \mathbf{u} = 0$) of a Newtonian fluid:

$$\rho \left(\frac{\partial \mathbf{u}}{\partial t} + \mathbf{u} \cdot \nabla \mathbf{u} \right) = -\nabla p + \eta \nabla^2 \mathbf{u} + \mathbf{F}, \quad (7)$$

where ρ is the fluid density, \mathbf{u} is the fluid velocity, p is the pressure, η is the dynamic viscosity and \mathbf{F} is the body force acting on the fluid. It can be rewritten in a non-dimensional form if we assume constant η :

$$\frac{\partial \mathbf{u}'}{\partial t'} + \mathbf{u}' \cdot \nabla' \mathbf{u}' = -\nabla' p' + \frac{1}{Re} \nabla'^2 \mathbf{u}' + \mathbf{F}', \quad (8)$$

$$Re = \frac{\rho L U}{\eta}, \quad (9)$$

where Re is the Reynolds number, L is the characteristic length, U is the mean velocity, $\mathbf{u}' = \frac{\mathbf{u}}{U}$, $p' = \frac{p}{\rho U^2}$, $\mathbf{F}' = \frac{L}{\rho U^2} \mathbf{F}$, $t' = \frac{U}{L} t$, $\nabla' = L \nabla$. Here, I also assume the flow velocity and the flow scale to be small; viscous forces dominate the dynamics of the fluid. That yields a small Reynolds number; this flow type is in general referred to as a creeping flow [3]. It simplifies the equation (7):

$$\nabla p = \eta \nabla^2 \mathbf{u} + \mathbf{F}, \quad (10)$$

$$\nabla \cdot \mathbf{u} = 0. \quad (11)$$

The flow described by Equation 10 is commonly called Stokes flow. The simplification is significant as we can use only a linear solver.

Comsol allows to implement these equations on the user level.

2.6.2 Dynamics of particles in liquid

After obtaining the electric field and the velocity field of the fluid, we can place particles into the medium and simulate their behaviour. Although DEP force is assumed to be the dominant force exerted on the particles in the micrometer scale, there are other observable forces significantly affecting the microparticles in a liquid.

Firstly, when an object moves through a medium it is damped. Due to the friction there is a drag force acting in the opposite direction of the movement. This force is proportional to the particle velocity and viscosity of the medium η . Thus, there is a terminal speed which can be achieved with a given force input. Obviously, the viscous drag is much more significant in liquids than, for instance, in the air and it depends on the shape of the object. For the simple case of a sphere

moving slowly through a fluid without turbulence, Stokes' drag can be applied:

$$\mathbf{F}_{\text{drag}} = -b\mathbf{v} = -6\pi\eta r\mathbf{v}, \quad (12)$$

where r is the radius of the sphere, \mathbf{v} is the velocity of the particle relative to the medium:

$$\mathbf{v} = \mathbf{u} - \mathbf{w}.$$

\mathbf{u} and \mathbf{w} are the velocities of the particle and the fluid respectively relative to the origin. Stokes drag model assumes:

- the objects are spheres uniformly composed,
- there is no turbulence in the fluid,
- smooth surface of the particles,
- and that there are no collisions among them.

Secondly, there is the buoyancy and gravitational force. Total force acting on a floating object in a fluid is:

$$\mathbf{F}_b = V(\rho_m - \rho_p)g, \quad (13)$$

where g is the gravitational constant, V is the volume of the particle and ρ_m and ρ_p are the densities of the medium and the particle respectively.

Thirdly, other important effect is Brownian motion. Brownian forces are random. Thus

$$\langle \mathbf{F}_r(t) \rangle = 0,$$

and average displacement from [18] is

$$|\Delta d| = \sqrt{\frac{k_B T t}{3\pi\eta r}},$$

where k_b is the Boltzmann constant, T is the temperature and t is the time. The effect increases with reduction of the particle size and becomes dominant for particles in nanoscale to the extent in which the manipulation using DEP is impossible. However, for the particle of radius $r = 25 \mu\text{m}$ in water of the room temperature, the displacement is on average over interval of one minute only slightly more than $1 \mu\text{m}$. That is small in comparison with the particle size and thus this effect can be neglected.

Additionally, there are various interactions among the particles which are important for modelling the overall behaviour of micro-particles in the liquid with more particles. They determine what will happen when two or more particles come into a closer contact. These

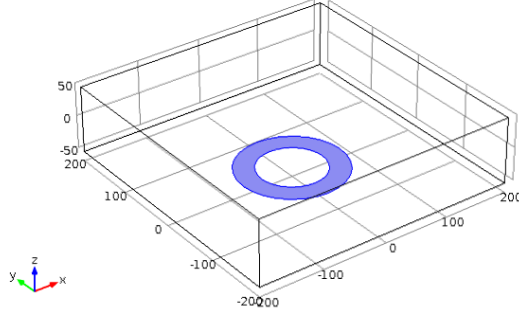


Figure 7: Image of the geometry built in Comsol with a sample circular pattern. At the bottom, there is a layer with adjustable conductivity and permittivity too thin to be distinguished in the image of the domain.

phenomena are encompassed in the *van der Waals forces*. Nevertheless, in order to design the *oiDEP* chip, the interactions among the particles are not crucial. In fact, only one-particle model can be illustrative enough.

There are other effects undergoing in the liquids with microparticles when electric field is applied such as *thermal flow*. The thermal flow is more than relevant effect in our application because we heat the fluid by both the electric current applied and the beamed light used for the electrode generation. The temperature gradients then result in the thermal fluid flow. Nonetheless, according to [36] the effect is even less significant than the Brownian motion for the optical intensities I used later in the experiments. Hence I did not consider this phenomenon either.

Finally, we can write the differential equation driving the motion of the particle:

$$m \frac{d^2 \mathbf{x}}{dt^2} = \mathbf{F}_{\text{DEP}} + \mathbf{F}_{\text{drag}} + \mathbf{F}_{\text{b}}. \quad (14)$$

The *DEP* force \mathbf{F}_{DEP} was already described above in Equation 1. The electroosmotic effect, which is in detail introduced in the section 2.3, enters into the equation through the drag component. Here, I make strong assumption that the flow is uniform past the sphere [3]. I also assume that the impact of the particles on the flow is negligible.

2.6.3 Geometry, materials and the boundary conditions

For the simulations I built a simplified geometry of the *oiDEP* chip. I made all the simulations only in an element with dimensions $400 \mu\text{m} \times 400 \mu\text{m}$ and $200 \mu\text{m} \times 200 \mu\text{m}$ since the behaviour is scalable. Figure 7 shows the geometry which imitates the projection of a circular image upon the chip.

The domain is 100 μm thick and is made of water; I used this thickness later in the experiments. At the bottom of the element there is a thin layer which is not visible in the Figure 7 as it is too thin in comparison with the whole element. The action of projecting image patterns is simulated by using a material with different electric properties in this layer.

The voltage is applied through the boundary conditions at the top and bottom of the element. The top wall is grounded while the side walls are modelled as insulators.

For the creeping flow, the side walls are treated as open boundaries while the speed at the bottom and top layer is determined by electroosmotic velocity boundary condition [11]:

$$\mathbf{u} = -\frac{\epsilon_r \epsilon_0 \zeta}{\eta} \mathbf{E}_T.$$

\mathbf{E}_T is the electric field tangential to the surface of the bottom layer, η is the dynamic viscosity of the fluid, ϵ_r is and ζ is the zeta potential of the surface. Zeta potential is the electric potential between the slip plane of the formed double layer at the surface and a point in the fluid far away from the interface. The value depends on the properties of liquid as well as on the properties of the surface. It usually ranges from -0.1 V to 0.1 V and determines the direction of the flow.

2.6.4 Parameters and material properties

It is impossible to obtain precise properties of the photoconductive layer because they significantly change with even a small change in fabrication procedure or simply by different treatment and storage. Usually it is even difficult to measure these attributes with high precision. Thus I chose only approximate values. In [35], conductivity of TiOPc is measured. Value of conductivity at the enlighten area σ_{light} was approximately $9 \times 10^{-6} \text{ S m}^{-1}$, while in the dark area σ_{dark} it was around $1 \times 10^{-10} \text{ S m}^{-1}$. Further, the relative permittivity ϵ_r of the organic materials as well as the organic polymers is assumed to be low. For example, [23] notes that relative permittivity of TiOPc $\epsilon_{r,\text{TiOPc}} = 3.9$. Nevertheless, other materials have different properties and therefore these values are only approximate.

On the other hand the properties of the liquid with microparticles used in experiments are well known. The dynamic viscosity of water η_w is 1.002 mPa s at 20°C . The relative permittivity of the deionized water used $\epsilon_{r,w} = 80$ while its conductivity σ_w , when measured during the experiments, fluctuated around $17 \times 10^{-6} \text{ S m}^{-1}$. Next, properties of PS are: $\epsilon_{r,PS} = 2.5$, $\rho_{PS} = 1.04 \text{ g cm}^{-3}$, $\sigma_{PS} = 1 \times 10^{-15} \text{ S m}^{-1}$.

The applied voltage $V_{pp} = 20\text{ V}$ while the frequency $f = 10\text{ kHz}$.

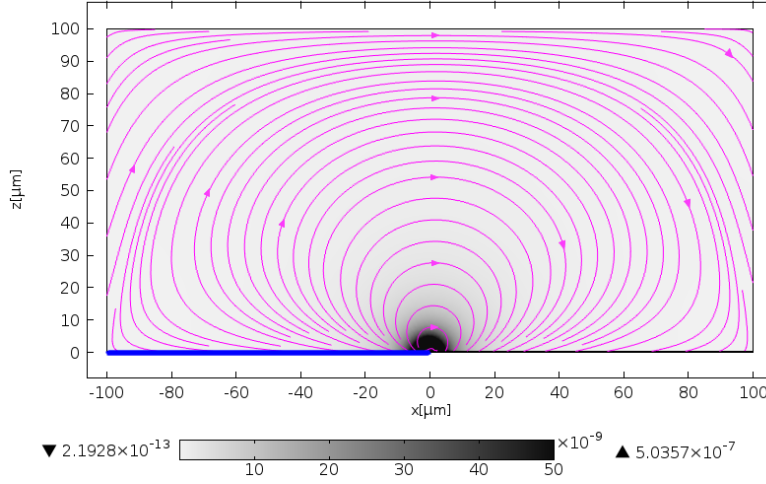


Figure 8: Total force field induced by the electric field for a single light interface. The shape of the field (streamline) and magnitude (surface) for thickness $0.3\ \mu\text{m}$, and $\zeta = -0.05\ \text{V}$ and $\sigma_{\text{light}} = 9 \times 10^{-6}\ \text{S m}^{-1}$. The electroosmotic flow is from the left to the right. The blue colour highlights the lit area.

2.6.5 Simulation results and discussion

Figure 10 shows the simulated shape of the total force field when two parallel virtual electrodes with distance $60\ \mu\text{m}$ and width $20\ \mu\text{m}$ are applied. Further, Figure 10d presents the possible trajectories of the PS particles with diameter $50\ \mu\text{m}$ placed within the field vertically in the middle of the chip. Trajectories are, of course, only illustrative because the model approximates the spheres by their centre of mass and does not restrict particle movement which would be in reality caused by their size. However, the damping corresponds with the size.

To trap a single particle, it is possible to use a hollow circle. The Figure 11 displays the force field shape for a circular trap with radius $40\ \mu\text{m}$ (see Figure 7) in a vertical view. The view is a cut in height $30\ \mu\text{m}$ of the chip.

In the vertical direction, the shape of the force field in Figure 10 suggests that the vertical manipulation is achievable since the PS beads should be repelled from the interface of the illuminated areas. In Figure 10d, the velocity in the vertical direction was around $700\ \mu\text{m s}^{-1}$. Meanwhile, the literature reports average velocities only up to $500\ \mu\text{m s}^{-1}$; see Table 1. The higher values in the numerical simulations are likely to be caused by too optimistic choice of the photosensitive material properties. Also, I made a number of simplifications which can cause an inaccuracy of the model.

For optimal manipulating force, we should keep the particle few micrometres away from the light interface. That resembles a surfer surfing on a tip of a wave. Like that, the particle will not be pushed

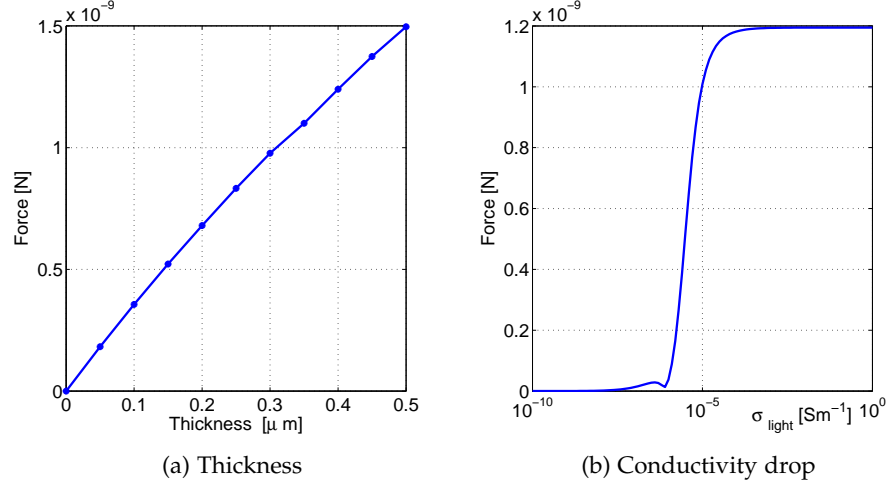


Figure 9: Dependency of the total force magnitude at the middle of the light-interface situation domain (see Figure 8) on (a) the total force magnitude on thickness, (b) the conductivity of the illuminated area σ_{light} . Meanwhile $\sigma_{\text{dark}} = 1 \times 10^{-10} \text{ Sm}$.

to the bottom of the chip. Hence, we could avoid the undesirable sticking. The simulations indicate that a range of the light interface is around $50 \mu\text{m}$.

According to the model, the most crucial parameters are the thickness of the photoconductive layer and the conductivity drop. They strongly determine the force exerted upon the particles. This is tested for the simple case of the light interface from Figure 8. Figure 9 examines the force magnitude at a point in the middle of the chip directly above the light interface, i.e. at $z = 50 \mu\text{m}$, $x = 0 \mu\text{m}$, depending on

1. the layer thickness in Figure 9a,
2. and conductivity of the illuminated area σ_{light} in Figure 9b.

While in the first case the dependency of the force magnitude is close to linear, in the second the characteristics rockets up at around $5 \times 10^{-6} \text{ Sm}$ by few orders and then it levels off. This confirms the importance of both the chosen photoconductive material and projection method.

In conclusion, the model helped me to grasp the concept of the [oiDEP](#) and offered me the basic insight into what should be happening.

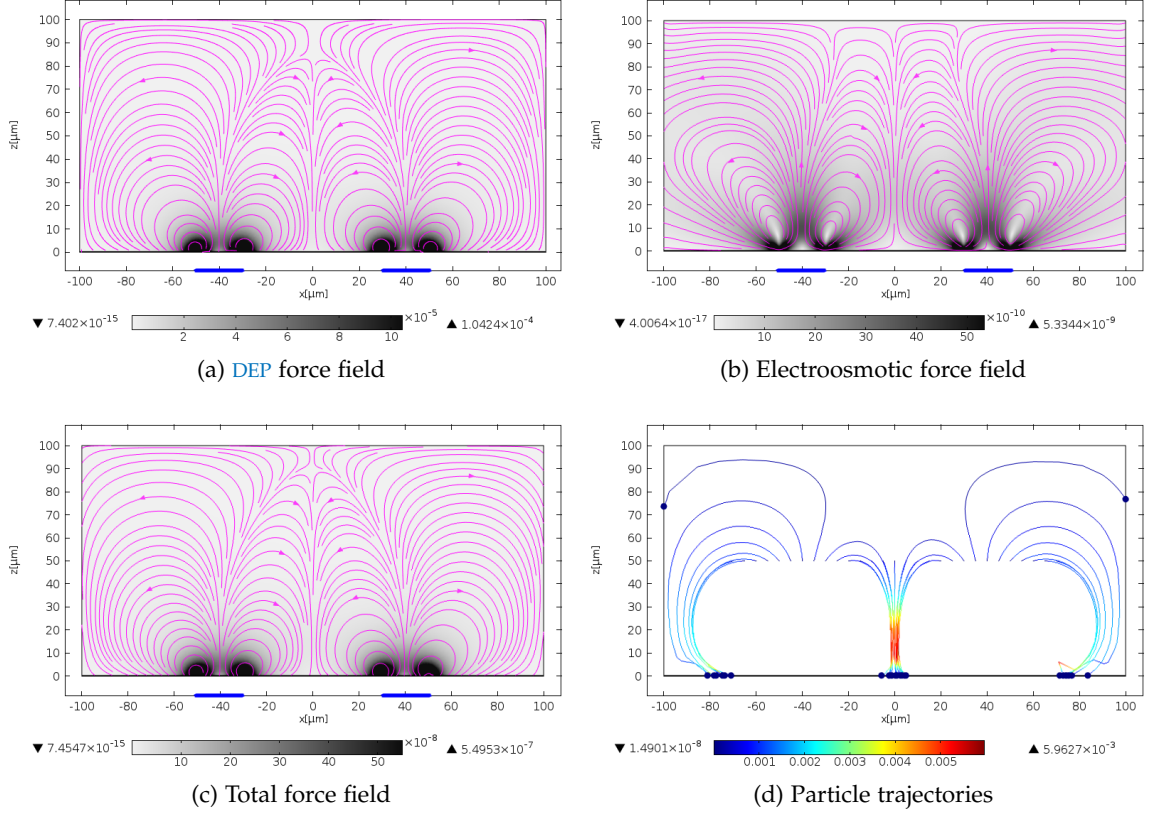


Figure 10: Force field shape (streamline) and magnitude (surface) within the oiDEP chip displayed in a vertical cut. It simulates two parallel virtual electrodes (highlighted by blue color). In (d), blue dots indicate the final position while lines depict the trajectory.

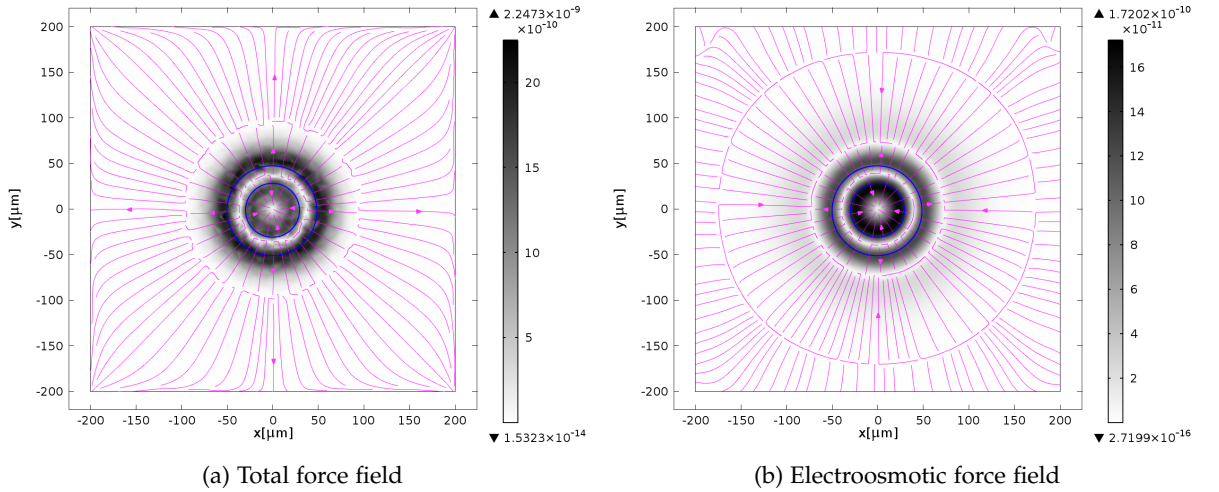


Figure 11: Force field shape (streamline) and magnitude (surface) within the oiDEP displayed in the horizontal cut in middle of the chip (30 μm). It simulates circular trap virtual electrode (highlighted by blue color).

OPTICAL FEEDBACK: USING A LENSLESS SENSOR

Visual feedback is a convenient method to determine the position of an object in the micrometer scale. It is a common practice in the laboratories to use a microscope. Yet, such complicated way requires a lot of space for expensive and fragile lenses.

The specific scale of the micromanipulation, i.e. the size of the objects and the area of manipulation, is comparable with the dimensions of the contemporary image sensors that are used in cameras. That allows placing an image sensor directly under the liquid with microparticles. When we use a proper light source placed against the sensor, the particles become distinguishable in the image thanks to their interaction with the incident light. That is natural for objects with size $50\text{ }\mu\text{m}$. However, by experiments I confirmed that particles as small as $5\text{ }\mu\text{m}$ can be located by the lensless sensor thanks to the diffraction effect.

Possible savings by replacement of a microscope from the feedback loop can be significant. In [chapter 5](#), I will show that the microscope, which is used as a feedback for automatic control, can be replaced by a cheap CMOS sensor without higher loss of precision. Only the price difference between the microscope and the lensless sensor is more than 65000 CZK.

Actually, this solution seems more favourable for the [oiDEP](#) because [oiDEP](#) already requires both the transparency of electrodes and the light source placed against the sensor. Moreover the electrodes don't have edges which turned out to be an issue when I used a translucent [MEA](#). I discuss that later in [chapter 5](#).

Finally, recognizing the diffraction patterns captured by the lensless sensor together with a good diffraction model gives us surprisingly more information than just position in a plane. Further, from the model we should be able to determine the position in the third dimension and distinguish two different particles.

3.1 IMAGE SENSORS

On the market there is a variety of options for the image sensing. Image sensors come with different dimensions, resolutions, intensity range and frame rate. Nowadays, there are basically two main methods used to convert light into the electric signals: CMOS and CCD image sensors. They don't have any distinguishable pros and cons for our application.

Besides that, new image sensor types has emerged recently. For example, in our laboratory we have access to so called Dynamic Vision Sensor (DVS) which was developed at ETH Zurich. DVS speeds up sensing by sending only the local changes at each pixel and thus allows very rapid sensing with high resolution. It is suitable for control of fast processes¹.

Nevertheless, for the first tests we opted for a cheap CMOS sensor on a chip Vimicro VCo345PLVAL dismantled from a USB webcam GRUNDIG 72820. The dimensions of the sensor are $1000\text{ }\mu\text{m} \times 750\text{ }\mu\text{m}$ while the resolution is 640×480 pixels; it is capable of a frame rate 30 fps. Thus the pixel pitch is around $1.56\text{ }\mu\text{m}$. The advantage of this solution is the simple implementation. There is no need of any other special programs or interfaces with the computer. It, however, did not offer any advanced functions like a frame rate control or access to the raw data. Additionally, the image from the webcam is already post-processed and compressed in JPEG.

3.2 EXPERIMENTS AND DISCUSSION

3.2.1 *Light source*

The light source is of a large importance. I tested various light sources. While I used only ambient light no particles were recognized in the signal from the sensor. The situation was similar with the source of coaxial light from a microscope. However, when a laser beam or a light from a high power LED was applied, patterns behind the microparticles occurred.

Figure 12 shows observed patterns behind 50-micron PS beads. At first I tested a collimated beam of light from 635 nm laser with adjustable intensity up to 2.7 mW. Secondly I used a high power white LED with intensity 30 cd/20 mA. For those sources I observed diffraction patterns as it is noticeable in the Figure 12. Obviously the diffraction was more pronounced for the laser light source.

There are two requirements on the light source I devised from the experiments:

- the intensity must be significantly higher than the intensity of the ambient light,

¹ At the moment, DEP perhaps doesn't exert forces of such degree that the use of DVS would be necessary. Though, the application area of the lensless image sensor is not limited only to the DEP manipulation. For instance, forces and thus even the particle velocities in the magnetic micromanipulation are significantly higher.

In fact, DVS has got a second feature which could be beneficial for the oiDEP device. In oiDEP the sensor captures an area of a projected pattern with the highest possible contrast. The principle of the conventional image sensors limits their intensity range captured in a single frame since all the photosensitive elements must be exposed at the same moment. Yet, each pixel in the DVS has independent gain and thus allows to capture images with very high contrast.

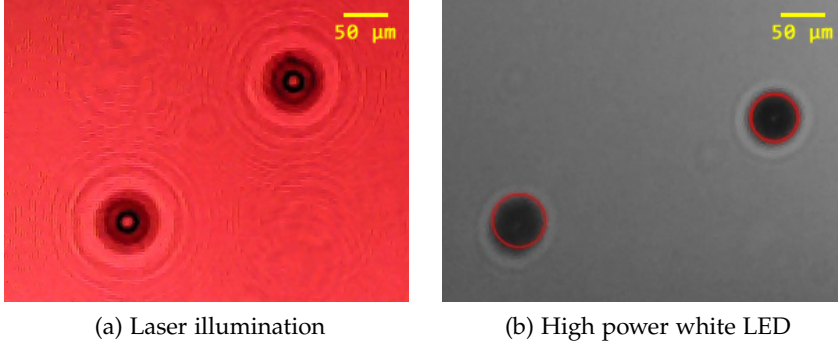


Figure 12: A cut from the image captured by the CMOS sensor with (a) laser illumination and (b) high power white LED. There are two 50-micron PS beads. Both images were captured under otherwise same conditions. The red circles are a result of a post-processing algorithm that located the particles. The algorithm is described in [section A.1](#).

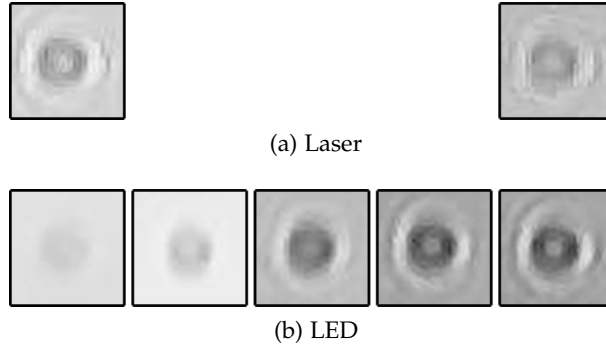


Figure 13: Image of a cluster of 4 yeast cells with total size around $10\mu\text{m}$ with (a) laser illumination, (b) LED illumination. It shows the pattern for source in distance 10 cm, 15 cm, 20 cm, 25 cm and 30 cm in an order from left to right. While for LED the change is significant, the effect is unchanged with the collimated laser beam.

- incident light rays should be parallel.

The second requirement can be treated either by a light collimator, by an increase of a distance from the light source (see [Figure 13](#)), or by obstructing the optical path by a slit. The latter two are a consequence of a point source property. When considering a point source we actually assume that light rays are parallel for the observer (our sensor). Only by creating a 0.5 mm slit for the LED used the image quality notably improved. It enabled mi to place the LED as close as 3 cm. The second requirement also explains why light from more sources, e.g. ring illumination, have only a negative effect.

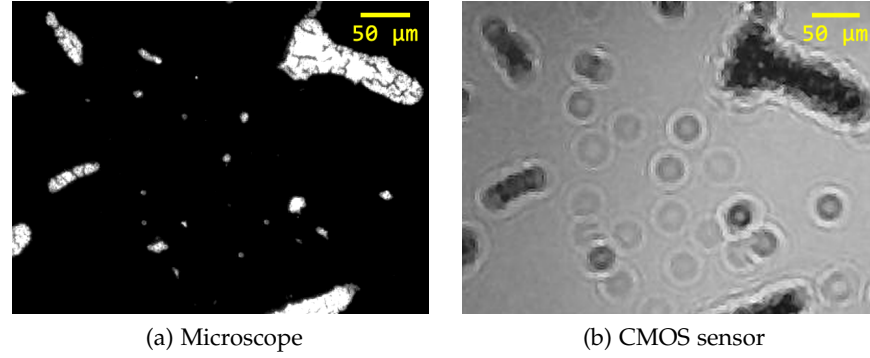


Figure 14: Yeast cells with size around $5\ \mu\text{m}$. The same scene was captured by: (a) microscope with $10\times$ lens, (b) a lensless sensor with LED illumination in distance 25 cm. It is a cut from less than a quarter of the area the CMOS sensor captures. Meanwhile it is a full image from the microscope. Notice that the separate cells can be easily located.

3.2.2 Yeast cells

It is feasible to use the diffraction effect to locate objects as tiny as $5\ \mu\text{m}$ when they are not clustered. This limit could be even improved by using a sensor with a smaller pixel size.

I demonstrated this on yeast cells; size of a typical yeast cell is around $5\ \mu\text{m}$. Figure 14 shows image captured by the lensless CMOS sensor with LED illumination and a microscope with $10\times$ Olympus lens. The LED was placed 25 cm above the sensor. The lensless sensor could cover area more than four times larger than the microscope. Single cells in the image from the lensless sensor are easily detectable and locatable. However, we cannot precisely distinguish individual cells in the clusters. Yet, it is possible to separate the clusters from the individual cells and for bigger clusters we can even detect the shape. With a proper model, we should be able to estimate the number of cells in the cluster.

A similar result can be achieved also with a laser illumination.

Additional problem to the clustering for the tiny particles is that they cannot be easily distinguished from the alien particles, e.g. from the pieces of dust, even in different focal plane. This could be also treated by the model.

3.3 LIGHT ABSORPTION AND SCATTERING BY SMALL PARTICLES

I prepared a model to predict scattering and absorption of light by small circular particles above the lensless sensor. The model is based on Mie theory. My main motivation was to explain the patterns of scattered light I observed on the CMOS sensor placed under the liquid with 50-micron PS spheres. The model predicts the light pat-

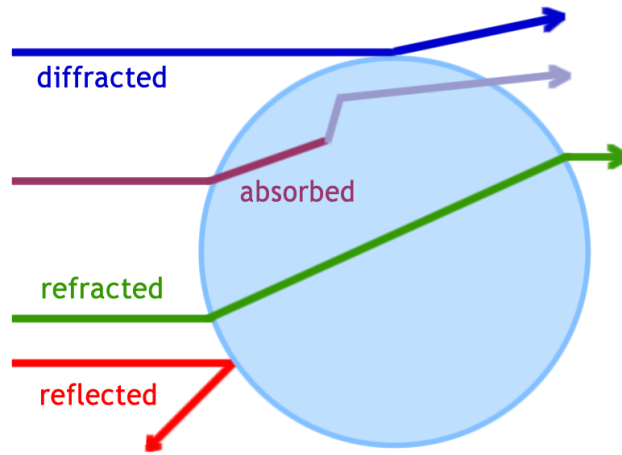


Figure 15: Diagram of the light interaction with spherical particles

terns for the particles with different optical properties and for different wavelength used in the light source.

This knowledge could be very valuable. For instance it allows to identify a particle that is in bulk with objects of other type or to determine a number of particles in a cluster. Also, in the future the model could be utilized for determination of the three dimensional particle position. That idea is inspired by [27], where Ovrzyn successfully used a similar model to measure velocity in three dimensions for seed particles following a flow in a thin channel. Velocity in the third dimension was determined just from the diffraction model. However, he used a microscope.

3.3.1 Light diffraction

There is a number of general effects when light interacts with a transparent spherical particle. Some of the light incident upon the particle may be reflected, refracted, diffracted, or even absorbed and then re-radiated (Figure 15). The extent to which these effects applies depends on the optical properties of the particle and the medium (radius of the sphere r , particle index of refraction n_p , medium index of refraction n_m). These properties then determine the patterns of high intensity light on the screen behind the particle where we place a photosensitive sensor.

Diffraction by edges, slits or particles is the result of scattering [2]. Besides that, scattering explains many other effects we come along in the everyday life. There is a host of applications of diffraction effect in industry and research².

² For instance, the effect of diffraction by particles is commercially used for precise size measurements. Particle size in the range from $0.1 \mu m$ to $8.75 mm$ can be determined when other optical properties are available; the method is known as *laser diffraction* and it has become a standard tool for this task in various fields [22]. In-

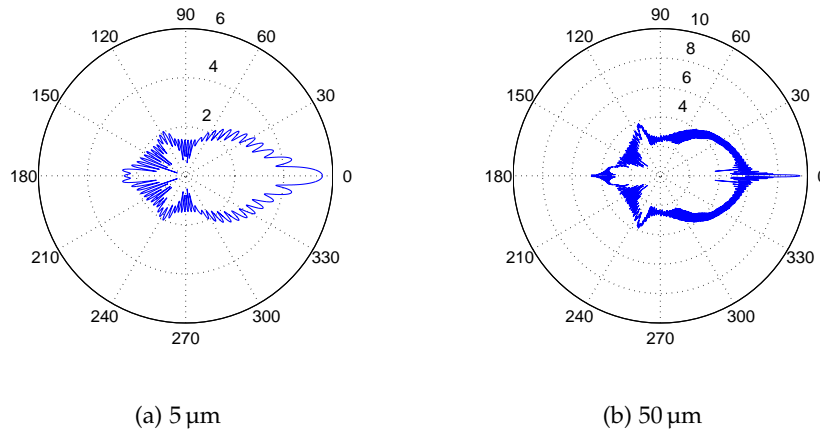


Figure 16: Simulation results of Mie scattering by a single PS sphere with diameter (a) 5 μm , (b) 50 μm immersed in water in the far field. Light intensity is in logarithmic scale closer to the human perception. The light is incident upon the particle from the angle 0° , i.e. from the left.

While smaller particles scatter the laser-light beam more intensely in greater angles, larger particles do so in smaller angles. Figure 16 gives sample characteristics. There, all the conditions but the size are the same. One can notice that most of the incident light for the larger particle is scattered in the forward direction. In addition to the size, the shape can be also analysed.

3.3.2 Mie scattering

To simplify the problem I assumed our particles, i.e. PS beads used in my experiment, to be perfect spheres.

Scattering by spheres is perhaps the most important soluble problem in the theory of absorption and scattering [2]. Mie solution of Maxwell's equation, which characterizes the scattering of electromagnetic radiation by a sphere, was published more than hundred years ago but remains of great interest to this day³. The model can be further extended for shell particles such as cells.

tensity of scattered light is precisely measured by light sensors. Then, based on a model of scattering, particle size distribution can be determined by correlation with the predicted values from the model.

³ Though, there is an alternative method feasible for opaque particles with size significantly larger than the incident wavelength and significantly different refractive index of the particle from the surrounding medium. Then, most of the light is scattered in the forward direction. Additionally, according to the Babinet's principle the diffraction pattern from a hole is identical to the one from an opaque body of the same size and shape. Therefore, if the stated conditions are satisfied Fraunhofer diffraction approximation gives sufficiently precise results. The benefit is that the calculations are much less demanding in comparison with the Mie model of scattering.

Essential contribution in this topic was made in [2]. Many programs solving the scattering by a sphere were created based on the ideas and propositions made by [2]. Most of them, however, gives only the far-field solution of diffraction from the object which is sufficient for most of the applications, for example the laser diffraction mentioned above. Figure 16 displays the far-field simulation results for 50-micron PS beads which I used in my experiments. However, I did not observe maximum intensity in the forward direction.

The liquid with the particles is placed upon a thin sheet of glass while the chip is directly attached to the glass. Thus the distance between the particle and the sensor is at most 3 mm. Therefore in my model I used near-field Mie calculations implemented in Matlab package MatScat developed in [33]. I make further simplification; values of the refractive index of the glass and water allows to omit the fluid-glass interface [27]. Therefore, the model gives us an approximation of the vector electromagnetic field directly on the chip.

3.3.3 Experiments and discussion

In my experiments, laser beam was used with wavelength 635 nm. 50-micron PS beads were immersed in deionized water with refractive index $n_m = 1.33$. The complex refractive index for PS microbeads was determined in [21]. The complex parameter is dependent on the wavelength; for 635 nm the value is approximately

$$n_s = 1.58 + i7 \times 10^{-4}.$$

Firstly, I simulated electromagnetic field intensity in three distances from the centre of the PS bead, in: 1 mm, 2 mm and 3 mm.

The simulations are compared next to each other with the experiment in Figure 17a. The image captured by the lensless sensor on the right was, of course, originally red because of the wavelength. I transformed the image into the grayscale afterwards for easier comparison. The images from the experiment, I carried out after the simulations, very well confirm the predictions.

Two basic patterns were observed from the same set of the particles, only with different distance from the sensor. The first one, displayed in Figure 17a, corresponds with the simulation in distance 1 mm. Further, Figure 17b displays the second one which corresponds with the simulation in distance 2 mm. The resemblance is indisputable.

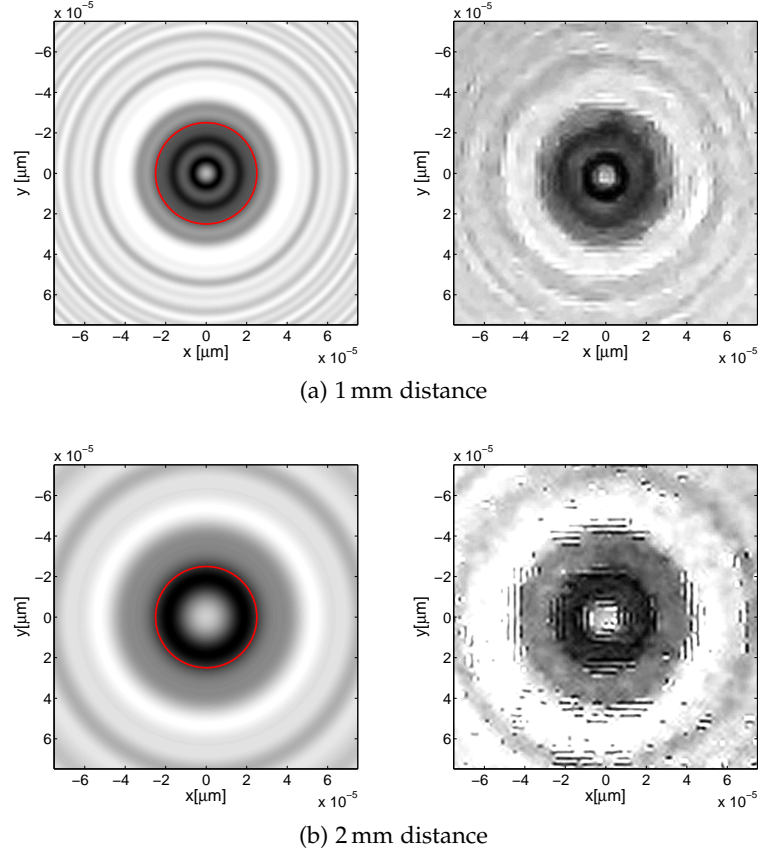


Figure 17: Diffraction patterns by 50-micron PS bead in detail. Computer simulation in distance 1 mm (a) and 2 mm (b) is on the left. The real pattern captured by CMOS sensor on the right. The black stripes are artefacts from high intensity.

DEVICE FOR AUTOMATIC MICROMANIPULATION BASED ON OIDEF

The ultimate goal of my thesis was to propose a design of a device which would be capable of fluidic micromanipulation using an electric field. In this chapter I combine the ideas discussed in [chapter 2](#) and [chapter 3](#), i.e. the [oiDEF](#) and the lensless sensor, into one device. Based on that I built a laboratory setup to verify the function. I was able to demonstrate first movement of 50-micron [PS](#) beads controlled by the projected image. I explain the experiments at the end of the chapter.

4.1 GENERAL SETUP

[Figure 18](#) outlines the essential elements of the device for micromanipulation. The block diagram describes a control loop. The [oiDEF](#) chip, in detail discussed in [chapter 2](#), is the core of the whole device.

In the first stage, the lensless sensor placed on top of the [oiDEF](#) chip, which is mounted in horizontal position, captures the image of the microparticles in the liquid. Here, I propose to use a lensless sensor but any imaging device capable of capturing the microparticles with sufficient resolution is suitable.

After that, the image is fetched to the computer, usually via Firewire or via more standard USB. An image post-processing algorithm then determines the position of the particles in the chip. From the position input, the controller subsequently generates image patterns. The image patterns are sent to the display device using a standard display interface such as HDMI, DVI or VGA. Finally, the loop closes when a particle changes its position because of the force caused by the incident light pattern on the chip.

Apart from the electrode shape, the controller might have the ability to change the frequency and amplitude of the applied voltage, light intensity and wavelength. In theory, that could allow proportional control of the exerted force.

4.2 OPTICAL SYSTEM

There are two basic requirements for the optical setup:

- the intensity and the wavelength of the incident light,
- pixel size.

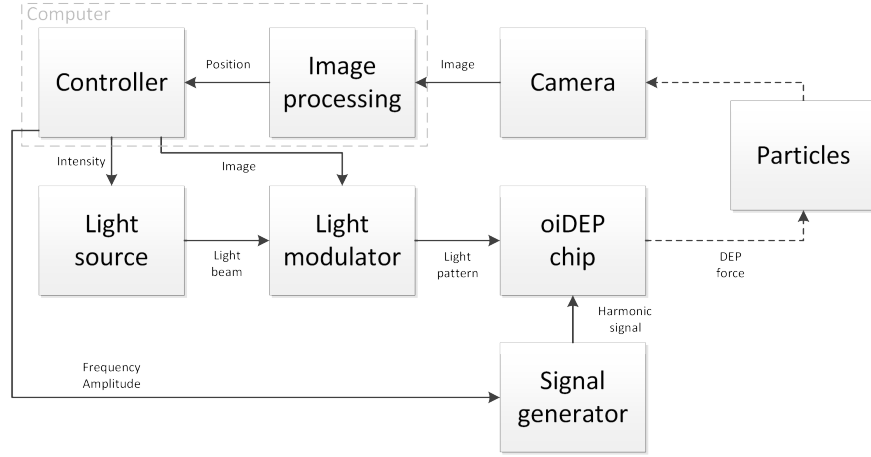


Figure 18: Block diagram of the device for automatic micromanipulation based on oiDEP principle.

The intensity and the wavelength is a critical factor solely determined by the material used in the photosensitive layer of the oiDEP chip. It influences drop in resistivity in the layer and hence the attainable speed of the particles; see section 2.6 where I modelled this behaviour. Absorption spectrum of the photosensitive material can suggest the most suitable wavelength for the light source. Some of the materials discussed above are mainly sensitive in the visible spectrum, others absorb mainly in the ultraviolet part of the spectrum. In case, that it peaks in the visible spectrum we can use of-the-shelf projectors.

The pixel size determines the attainable detail of the projected shapes. The smaller the pixels are, the more freedom in the control we have. The goal was to move the cells and beads ranging in diameter from $5\text{ }\mu\text{m}$ to $50\text{ }\mu\text{m}$. It would be very reasonable to be able to create an electrode maximally half of the controlled particle size. Therefore, the target pixel size was $2.5\text{ }\mu\text{m}$.

4.2.1 Display technologies

The first option to control the intensity upon the oiDEP chip appears to be LCDs. However, it is still a challenge to achieve such pixel pitch without any optics. For instance, popular high resolution retina display have pixels with 80-micron distance. Moreover, the conventional LCDs with built-in back light are unsuitable as they are made to offer wide viewing angle. That would cause fuzzy virtual electrodes and undesirable current leakage. Nevertheless, there were some partly successful tests when additional optical elements (condenser lens) were added [19].

Because of the pixel-size requirement I opted for image projection so that additional optics could be employed. Currently, there are three main methods used in the modern projectors to modulate light

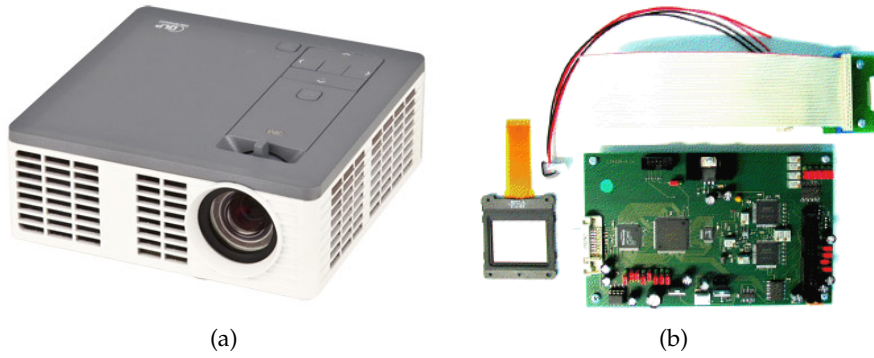


Figure 19: Photos of used optical devices: [DLP](#) microprojector (a) 3M MP410, (b) OEM kit Holoeye HEO 0017.

- liquid crystal ([LC](#)) modulators, [DLP](#)¹, and finally liquid crystal on silicon ([LCoS](#))².

At the end, we decided to test two different approaches. A [DLP](#) out-of-the-shelf microprojector and a spatial light modulator using liquid crystals were purchased. While the first is a cheaper solution, the latter, although very expensive, offers more freedom. We can use it to modulate arbitrary source of light, for example available laser with 635 nm wavelength. Hence it is adaptable to the parameters of the photosensitive material ([subsection 2.5.1](#)).

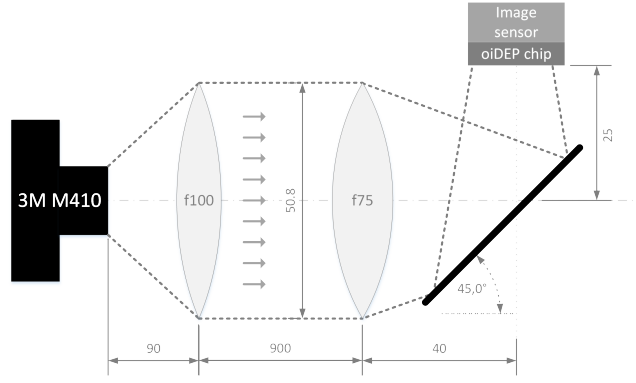
4.2.2 Projector setup

A microprojector 3M MP410 with extraordinary brightness 300 lm and resolution up to 1920×1080 pixels was used ([Figure 19a](#)). I used HDMI for the connection with a computer. I added two 2-inch convex lenses purchased from Thorlabs. While the first lens placed directly behind the projector lens was meant to collimate the emanated beam, the second lens reduced the image size. Finally, I added an ordinary mirror to bend the image upright as the [oiDEP](#) chip must be in a horizontal position. The microprojector setup used is sketched in [Figure 20a](#). The sketch includes measured distances between the lenses. With that I achieved pixel size around $2.5 \mu\text{m}$ and slightly distorted image. By increasing the distance between the two lenses, the pixel size would reduce even more.

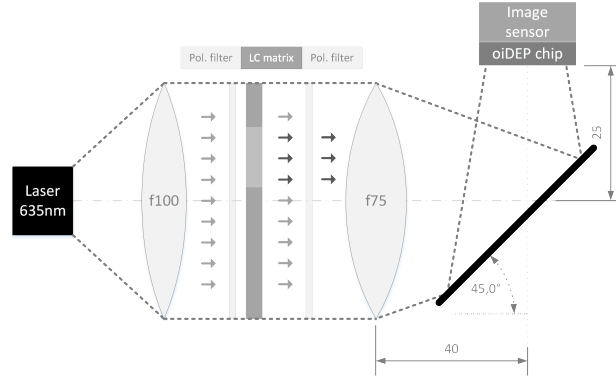
The optical path could be improved and the degree of magnification increased if I removed the internal lenses. For that, of course, I would have to dismantle the projector.

¹ [DLP](#) is very interesting technology using extremely fast micro-mirrors that reflect source light on a screen.

² [LCoS](#) is similar to the [DLP](#); only the liquid crystals are used instead of the micromirrors to control the reflection of the incident light.



(a) DLP microprojector optical system.



(b) Spatial light modulator optical system.

Figure 20: Optical systems with the DLP microprojector and the light modulator. The dimensions are in mm.

The projector achieves the feeling of colour projection by fast switching between different colours. That is, however, unfortunate for both - the optical feedback and the oiDEP. Firstly, higher shutter speed for the image sensor must be used since it would have otherwise caused blinking due to the different frequency of colour change and shutter. This effect made the combination of our image sensor and the projector unusable. We could not set sufficiently slow shutter speed for the sensor. Secondly, the switching between wavelengths and intensities could have unpredictable effects on the photosensitive layer.

4.2.3 Spatial light modulator optical setup

Additionally to the microprojector, I tested a twisted-nematic LC based device to modulate a beam from a laser light source. I used an OEM kit Holoeye HEO 0017. The OEM kit is based on a commercial display from Sony with dimensions $36.9 \text{ mm} \times 27.6 \text{ mm}$. There is 1024×768 active pixels in the LC matrix. The kit allows only DVI connection with a computer.

The layout with the spatial light modulator resembles the previous setup. It is depicted in [Figure 20b](#). Laser beam is brought in by an optical fibre. The LC matrix is added in between the two lenses. Also, two external polarization filters are placed in front and behind the matrix. The filters are arranged along perpendicular polarizing axis. Similar composition to this is in a smaller scale used in some projectors.

I used Fabry-Perot Benchtop Laser Source with intensity up to 2.5 mW and wavelength 635 nm. The final image at the [oiDEP](#) chip was corrupted by diffraction patterns from the LC matrix; see [Figure 24b](#). The diffraction arises from the LC elements of the modulator. Each element behaves like a slit in a diffraction grating. Firstly, the images repeat periodically, and secondly they are deformed. Also the background is not uniform, we can observe a squarish pattern. See [Figure 24b](#).

In the final experiments, I omitted the first lens for the beam collimation for practical reasons. Like this I was free to switch between the projection methods in price of the impaired magnification and intensity. Pixel size was approximately 6 μm . However, because of the diffraction the projected pattern must have had size at least 10 px to be visible. Also the front polarization filter could have been left out because the output from the used laser source is already polarized.

4.3 SOFTWARE

In the [oiDEP](#) device, a computer is the essential element which links the sensor, user and the display device. Computer program acts as a controller, it generates images which are then sent to the display device.

I developed two programs in Java specially for the [oiDEP](#) device to control the particle movement. While the first program implements the automatic object position control, the second one serves as a handy tool for manual control. It simplified the initial testing of the concept.

Both programs are adjusted for the two-display setup. That allows the user to place a small control panel on the main display while on the light modulator, which is treated by the operating system as a second display, a frame in a fullscreen mode displays the control outputs. Meanwhile the user can perform other tasks on the main display like checking the camera output.

4.3.1 *Software for manual control*

The manual-control program is only a simple utility which enables the user to create arbitrary shapes from elementary images and then swiftly adjust them. It is in detail described in [section A.2](#).

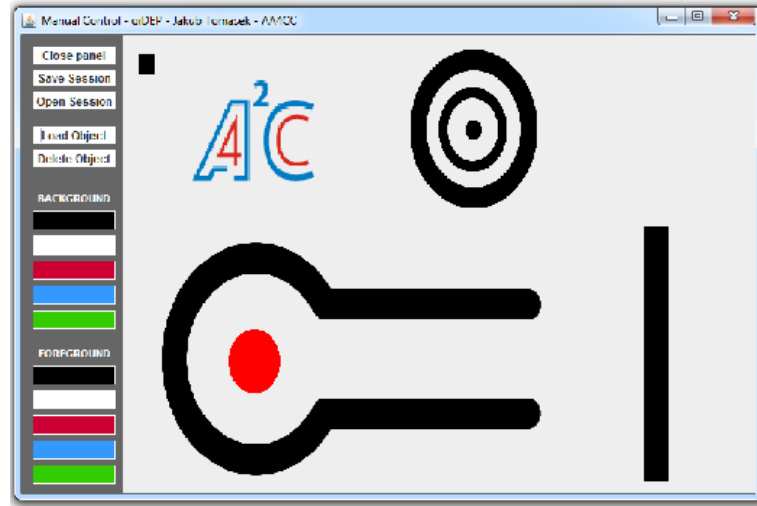


Figure 21: User interface of the manual control program with sample objects.

4.3.2 Software for automatic control

On the other hand, the program for automatic control is more complex. From the beginning, I aimed for multiple particle manipulation. Firstly, it processes the input image fetched from the sensor. It recognizes the objects and determines their position. The particle recognition is based on the Hough circular transform. The crucial function of the program is then to keep a track of the particles.

The GUI enables the user to set a goal location for each particle separately; see Figure 22. A simple A* and local repair A* (LRA*) ensures to find the shortest path possible at each step of the algorithm. Ultimately, it generates the image patterns which control the location of the particles according to the position of the particles.

All the steps of the algorithm I developed are encompassed in [section A.1](#).

4.4 LABORATORY SETUP

I built a laboratory model of the [oIDEF](#) device depicted in [Figure 18](#). All the main parts of the setup were already covered in [sections 2.5, 4.2, 4.3](#) and [chapter 3](#).

4.4.1 Optical feedback

In the experiments I aimed to employ the CMOS sensor examined in [chapter 3](#) placed on the chip Vimicro VC0345PLVAL. The chip connects with the computer via USB. However, for the initial testing it was more convenient to use a monochromatic microscope composed

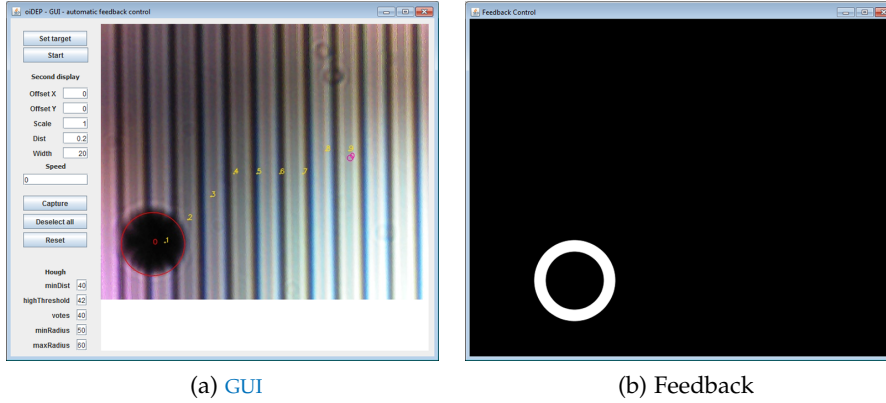


Figure 22: The program recognizes a 250 μm bead. The user used GUI (a) to input the target position (purple). The yellow path is computed by A*. (b) illustrates sample generated circular trap based on the (a). The image should be forwarded to a projector and displayed on the oiDEP chip. Its width, distance from the particle, coordinates can be altered by the settings in the GUI. On the background, there is a MEA from the chapter 5.

from a camera Pike F-032 by Allied Vision and Olympus $4\times$ lens. The camera is interfaced with computer via IEEE 1394b.

4.4.2 oiDEP chip

Additionally to that, I assembled a special mount for the oiDEP chip. The mount allows an easy disassembling of the chip and 3D manipulation in reference to the incident light. Like this I could ensure that the projected image upon the chip is sharp by vertical displacement and I was able to swiftly change the area of manipulation by displacement in the horizontal plane. The picture of the mount is in Figure 23a.

Figure 4 pictures very well the oiDEP chip layout I used. The layout is only slightly adjusted for the mount. A scotch tape with a thickness 100 μm is attached to the upper electrode; it keeps the distance between the two sheets of glass. While the position of the upper sheet is adjustable in vertical position, the the bottom sheet with the photosensitive layer is firmly attached to the construction. A small amount of the liquid with the microparticles is then placed on the bottom sheet. It reminds a vice, see Figure 23a. Finally, the upper sheet is pushed towards the bottom sheet with the microparticles in a fluid placed on the photosensitive layer.

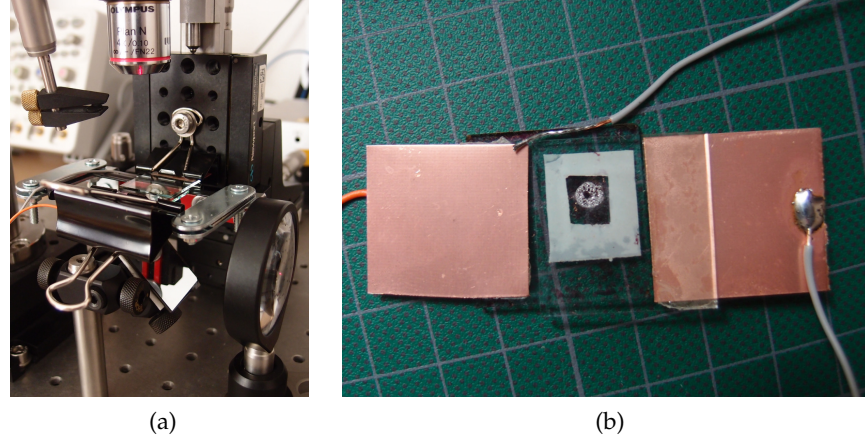


Figure 23: (a) shows the oiDEP chip fixed in a precisely-positionable mount. The mount is placed under a microscope. Also the mirror and second convex lens is visible in the picture. (b) The second option to create the oiDEP chip apart from the mount in (a) is to stack the sheets together by a double-sided tape.

4.4.3 Signal generation

The applied signal was generated in an arbitrary waveform generator Agilent 33220A. Although I controlled the generator manually, control from computer is possible. To ensure a good interface in between the generator and the oiDEP chip, planar Cu electrodes are attached on the edge of the ITO sheet by a double-sided conductive tape.

While the applied harmonic voltage was 20 V peak to peak, the output of the generator was set for high impedance load. I tested various frequencies; the frequency ranged from 1 kHz to 1 MHz.

In the experiments I used exclusively PS microbeads with diameter $50\text{ }\mu\text{m}$ immersed in the deionized water with conductivity ranging from $17 \times 10^{-6}\text{ S m}^{-1}$ to $50 \times 10^{-6}\text{ S m}^{-1}$.

4.5 EXPERIMENTS AND DISCUSSION

4.5.1 Image quality

Figure 24 shows a cut from a captured image for both light sources. There, only sample images are projected on the chip to illustrate the projection quality. With the projector setup I obtained very sharp image with high detail. One pixel was around $2.5\text{ }\mu\text{m}$. The image projected by the modulation of the laser light was worse due to the diffraction on the LC matrix while the pixel size was around $6\text{ }\mu\text{m}$.

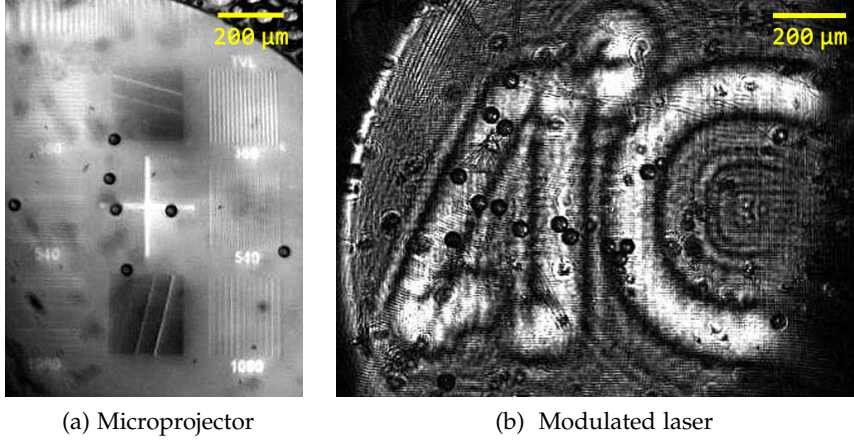


Figure 24: Patterns projected by the two setups on the *oiDEP* chip with 50-micron PS beads. The images were captured by a microscope. (a) displays LCD monitor test pattern; the image is sharp and very detailed. The pixel size was around $50\text{ }\mu\text{m}$. In (b), logo of AA4CC is projected by modulation of laser beam using the LC beam. The image is impaired by diffraction.

4.5.2 Polymer layer

For the first tests I had only four ITO sheets coated with the polymer layer available; they are denoted X1-X4. See subsection 2.5.1 where I discuss the materials more in detail. Unfortunately, the electrical properties of the polymer layer deteriorate due to the oxidation. Thus the sheets were kept in an inert atmosphere box up until the experiment.

Resistance of the oiDEP chip

When the chip was assembled together with the sample X3 I measured the resistance in between the ITO electrodes, i.e. the resistance of the polymer layer together with the layer of deionized water. I illuminated the whole *oiDEP* chip with light generated by a projector. When dark, the resistance was around $7\text{ M}\Omega$. The resistance for the illuminated chip differed with the wavelength. While for blue and red colour it was around $1.5\text{ M}\Omega$, for green light it was almost twice higher, i.e. around $2.8\text{ M}\Omega$. That could be caused by the absorption spectrum of the sample X3; see Figure 6. Yet, it can be also caused by different intensity of the LEDs embedded in projector.

Polymer layer peeling

There was a problem with the fabricated polymer layer. The layer coated on the ITO sheet was very fragile and after a few experiments it peeled off and adhered to the top sheet. Figure 25 displays both sheets after a few experiments. The hypothesis is that the PEDOT:PSS

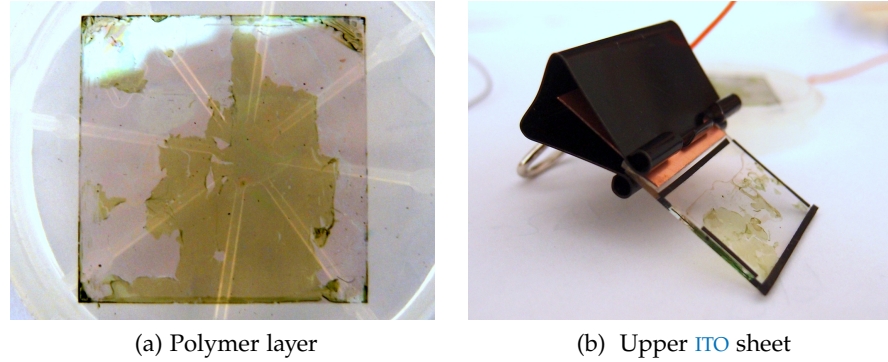


Figure 25: The upper ITO sheet (b) is pushed towards the bottom sheet (a) with the microparticles in a liquid. After several experiments a part of the polymer layer plucked off and adhered to the upper layer in (b). (a) shows damaged polymer layer.

layer, which is placed in between the ITO layer and the $P_3HT:PCBM$ layer, dissolves in the water used in the experiments due to some initial surface irregularities of the upper layer. The $P_3HT:PCBM$ layer then starts to float and tears apart due to adherence. In the future we will test a layout without the $P_3HT:PCBM$ layer.

4.5.3 Particle manipulation

I included several videos on the attached CD which captures the experiments. However they do not show such sharp patterns. The patterns more remind a stain. That is caused by a blow-out on the camera chip as the projected pattern has a huge contrast. The contrast is required to induce the motion. When the projector was used I must have set a slower shutter speed, otherwise blinking occurred in the signal due to the change in synchronization of the camera shutter with different colour cycles of the projector. To correct this I had to add an absorptive filter on the camera lens. That wasn't however sufficient.

Finally, I didn't achieve full manipulation but I observed forces exerted on the particles in consequence of the light modulation. The force is most likely the DEP force predicted. The first video in the included files shows a movement of a particle when a circular pattern approaches; see Figure 26a. The particle is repelled from the edge of the circle. Such behaviour however couldn't be observed for every particle during all the experiments. The DEP force induced by light shifted the particle approximately by $50\mu m$. Meanwhile the particle tended to return to the original spot. That is likely caused by the shape of the field since the particle was placed at a spot where the polymer layer was thicker. In Figure 26a the thicker layer is darker.

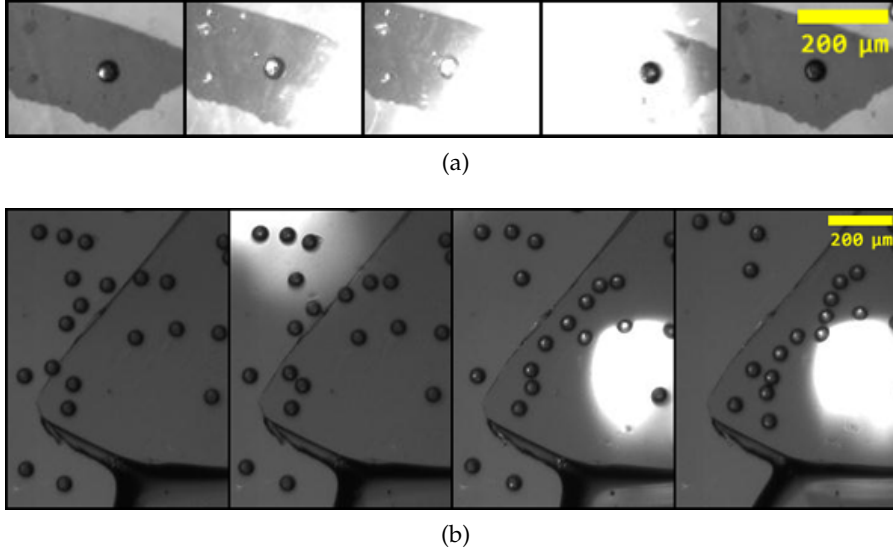


Figure 26: Image sequence from the experiments. (a) shows movement of the particle induced by the light pattern. In (b), particles move perpendicularly away from the interface of the area with and without the photoconductive layer.

This also suggests that the layer used was too thin to create sufficient inhomogeneity.

In general, I observed very strong forces when the voltage was switched off and on; they were likely caused by inhomogeneity of the material. Yet, that was only local. Further, sometimes I could observe a slower steady movement towards one direction of single particles in bulk. I could not explain this behaviour.. It could again have the origin in some impurities in the photoconductive layer.

There is a large number of unknowns. However, based on the experiments I could verify that the [oiDEP](#) chip is constructed correctly and the electric field is strong enough to move the particles. [Figure 26b](#) shows a movement of particles on the borderline of the area with and without the polymer. Meanwhile they do not seem to react to the light. The particles move perpendicularly to the border into the area with the polymer. In fact, this even confirms the predicted behaviour by the model in [section 2.6](#) because the area with the polymer has higher resistivity than the area without the polymer. The latter emulates illuminated polymer layer. The particles were repelled from the area to a distance around $60\text{ }\mu\text{m}$ and they moved with an average velocity above $10\text{ }\mu\text{m s}^{-1}$.

Hence, I conclude that either the polymer layer is too thin or the incident patterns do not create sufficient contrast to excite the layer and create the inhomogeneity. [oiDEP](#) chip with thicker polymer layer will be tested in the near future. In the next experiment I will also try to minimize the ambient light. I could also try to use laser light with different wavelength and higher intensity.

TRANSLUCENT ELECTRODE ARRAY WITH VISUAL FEEDBACK

During my work I tried to verify that it is possible to utilize the lensless CMOS sensor with the [MEA](#) setup currently successfully used for micromanipulation. To demonstrate that I adopted a functional feedback controller designed for an opaque array and a microscope composed from an industrial camera with attached microscope lenses. The controller was based on a preceding work by Jiří Zemánek [42].

This solution brings further simplification of the instrumentation by replacing the camera and the microscope lenses with a simple and inexpensive CMOS sensor. For instance, the price difference of the Pike F-032, the cheapest solution of the company Allied Vision available with a microscope mount, with mounted Olympus lens and microscope stand purchased from Edmund optics, and a cheap CMOS sensor extracted from a webcam is more than 65000 CZK. If the full microscope was used the price difference would be even more significant.

5.1 TRANSLUCENT MICROELECTRODE ARRAY: ITS FABRICATION AND DESIGN

The array design is based on the previous work done at [AA4CC](#). The amplitude difference between parallel electrodes creates the non-uniform electric field and induces the [nDEP](#) force acting on the [PS](#) bead immersed in deionized water.

Transparent electrodes are deposited on a circular sheet of glass with diameter 100 mm. Electrode pattern is fabricated by employing the standard process of lithography. The material of electrodes is [ITO](#) which was also exploited for the fabrication of the transparent planar electrode in the [oiDEP](#) chip described in [chapter 2](#).

The [MEA](#) prototype was designated only to verify the technology. Thus, we opted for a simple electrode pattern allowing manipulation only in one direction. Nevertheless, basically arbitrary composition is possible; it is limited by the fabrication process and space for interface. The design of the array is depicted in [Figure 27](#). In total, there are four sets of different electrode sizes with eight electrodes in each set. Meanwhile each two sets are connected and thus dependent. The spacing of electrodes is equal to their width: 100 μm , 50 μm , 20 μm and 10 μm for the widest electrode.

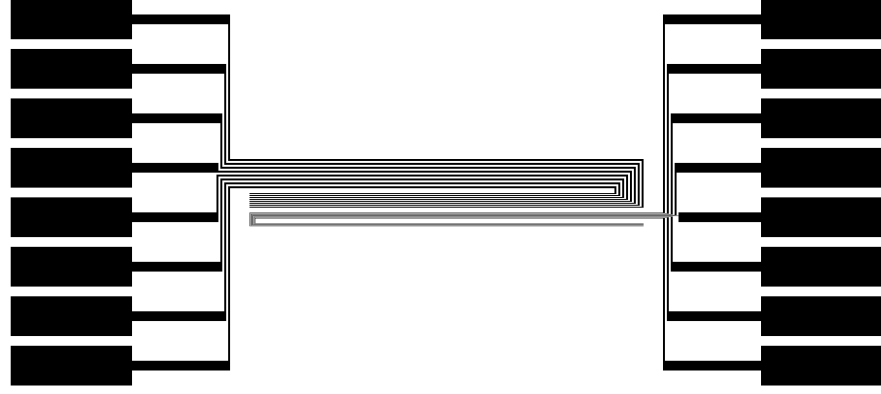


Figure 27: The layout of the electrodes of the transparent MEA.

5.2 EXPERIMENTAL SETUP

I used a thick Polydimethylsiloxane (PDMS) layer, which was stuck by an adhesive force to the sheet of glass, to create an open pool above the electrodes. The pool is designed to hold the liquid with the microparticles. For the manipulation I used deionized water and 50-micron PS beads. The pool with the liquid can be seen in Figure 28b.

An arbitrary waveform generator generates a harmonic signal with the desired frequency. A bipolar amplitude modulators then adjust the signal phase for all eight electrodes separately. The modulators are controlled from Matlab environment using a PCI data acquisition card Humusoft MF-614. Finally, the signal is interfaced to the MEA using test clips from 3M.

Most importantly, a lensless CMOS sensor fetches the image of the area of the interest to the computer. A chip with the sensor was mounted under the array as close as possible. Additionally, a high-brightness LED with intensity 30 cd/20 mA is placed 3 cm above the array to illuminate the microparticles.

In parallel to the CMOS sensor, the particles and the electrodes were also observed by microscope to verify and to compare the captured image.

The whole platform is placed on a damped table in order to cancel the disturbances from the environment. Figure 28a outlines the whole setup. Notice that while the microscope occupies almost the whole image, the chip with the sensor mounted under the array is almost unnoticeable.

5.3 CMOS SENSOR

I used a cheap sensor on Vimicro VC0345PLVAL extracted from the webcam Grundig 72820. The dimensions of the sensor are $1000\text{ }\mu\text{m} \times$

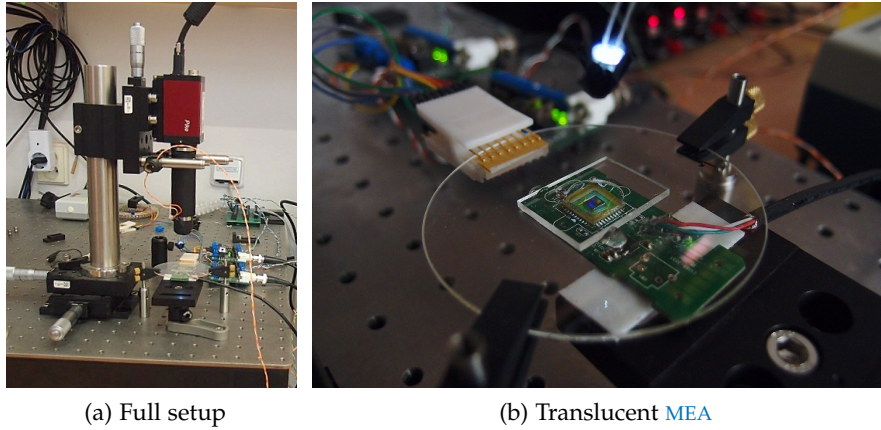


Figure 28: Translucent micro-electrode array experimental setup. In (b), the MEA is connected to the generator. Also the LED illumination is visible.

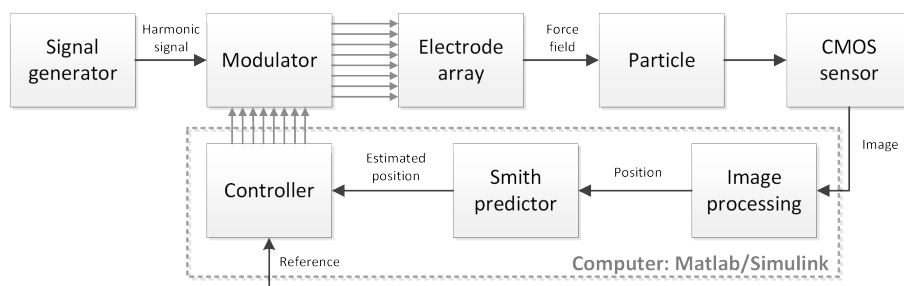


Figure 29: Diagram of the experiment with the translucent micro-electrode array.

750 μm with maximum resolution 640×480 pixels. Hence 1 pixel is square with edge length 1.56 μm .

The chip allows simple USB connection to the computer. Since Image Acquisition Toolbox supports the webcam the feedback is instantly ready to be used with the Matlab environment.

5.3.1 *Illumination and light diffraction by electrode edges*

Unfortunately, the illumination of the scene is not arbitrary. While for the microscope there are usually no special requirements for lighting, for the lensless sensor the choice is limited and affects significantly the quality of the image. The goal is to create a distinguishable differences in the amount of light incident upon the chip behind a particle due to its interaction with light, i.e. due to diffraction, reflection, refraction and absorption on the particle. I reported some viable illumination methods in [chapter 2](#).

At first, I tested a laser illumination with wavelength 635 nm (red). Without electrodes the laser illumination was advantageous as the higher degree of diffraction, i.e. the contrast and wide reach of the diffraction patterns, allowed locating even the small particles easily. However, here not only the particles diffract the light but there is additional diffraction by the electrode edges. That completely prevents a precise location of the particles. [Figure 30a](#) displays the obtained image of the area with three 50-micron [PS](#) beads. Even a human has troubles to distinct the particles. Notice that there is more stripes than electrodes. Thus, it does not even allow us easily find the electrode position in the image which is also crucial.

Further, coaxial light used in microscopes was unsuccessfully tested.

Finally, a simple high-brightness LED with restricted emission angle by a pinhole yielded the best results. [Figure 30b](#) shows the coloured image from the sensor. Beads with 50 microns in diameter are now easily located. This can be additionally improved by indirect illumination; that way the beads are more blur but, on the other hand, the dark stripes disappear completely. It proved to be the most favourable conditions to obtain precise position for the image processing algorithm. [Figure 28b](#) shows the light source placed above the array with microparticles and a liquid.

5.3.2 *Image processing*

The image obtained from the sensor is processed to attain position x of the object entered by a user.

When using the microscope with a ring light, the [PS](#) beads on the array are distinguishable as bright circles on a dark background. Image of the bead captured by the microscope is in [Figure 31c](#). Thus original recognition algorithm implemented in Simulink uses segmentation to

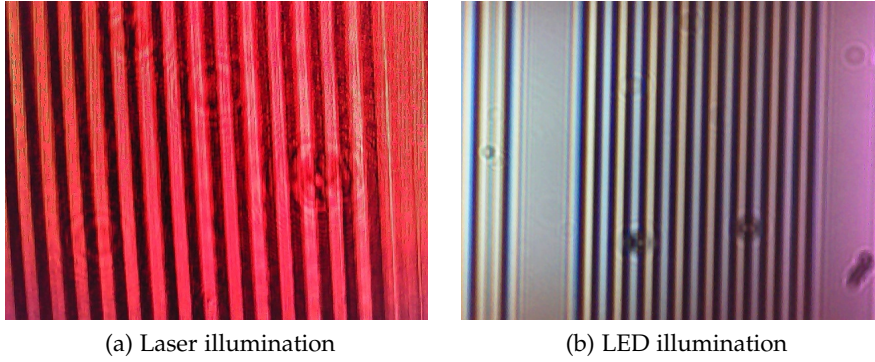


Figure 30: Image of the electrodes and PS beads with diameter $50\mu\text{m}$ from the CMOS sensor with (a) laser illumination, (b) LED illumination. While in (a) the beads are hardly distinguishable, the situation in (b) is better. In the latter, there is 8 electrodes in total; their centres are yellow.

remove the electrode edges and noise in the background. Position of the bead is then determined by finding the centre of intensity using image moments in an area that the user chose.

However, when using the feedback from the CMOS sensor the beads are dark on a bright and dark background; see Figure 30b. Therefore I refined the original algorithm by an additional step. After image acquisition, the algorithm during the initial processing step subtracts the image from the background. Now, added particles glow on the black background. Figure 31 illustrates the radical improvement. This image is then fit to be processed with the algorithm proposed for the original setup.

At the moment, the image of the background is taken during the initialization step. This solution is prone to fail when ambient light changes. That can be of course avoided by covering the whole platform. To avoid this bottleneck completely an extension is possible; we could adjust the image of the background at every step of the algorithm.

The advantage is that there is no problem with the dirt and impurities on the image sensor or the MEA. It is quite useful since the fragile electrode layer shouldn't be cleaned. Moreover, this helps with the problem of non-uniform illumination on the scanned surface.

For this step, I also added a support for multiple objects tracking.

5.4 CONTROL LAW

The goal is to control the particle position. Based on the real position relative to the reference, electrodes are switched to repel the microbead towards the goal.

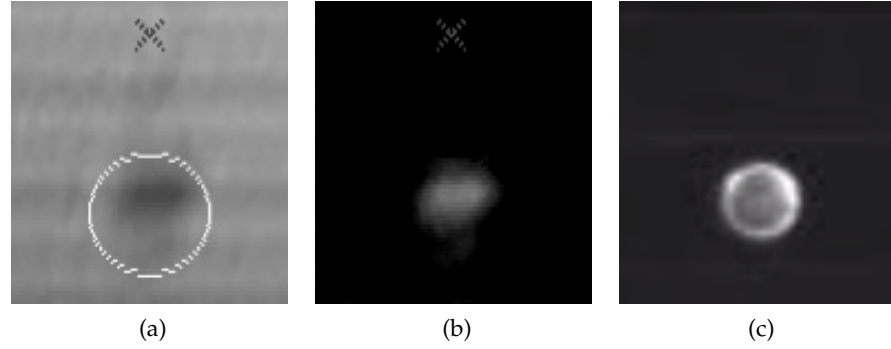


Figure 31: (a) shows a detail of the original image captured by the CMOS sensor compared with the processed image in (b). The white circle highlights the particle in the first image. During the image processing, background is subtracted from the original image. Then the particle glows on the black background. Additionally, (c) displays the image from the microscope with a ring light illumination.

Additionally, Smith predictor is employed in order to compensate the delay by the instrumentation and the position computation. Smith predictor computes the real position based on the delayed information and the model of the system. Thus, in my work I had to refine the model of the new electrodes and alter the delay.

The control law is in detail described in [42]. Please refer there for further information. Algorithm is implemented in Simulink environment in Matlab.

Besides that, we proposed a method to independently control multiple particles on this interdigitated array; see [Appendix B](#).

5.5 RESULTS AND DISCUSSION

5.5.1 Precision of particle position measurements

The main task was to verify whether a lensless CMOS sensor could be used as a cheaper alternative to the microscope in order to measure position of an micro-objects immersed in a liquid. As I mentioned earlier, additionally to the sensor there was a microscope capturing the same scene as the sensor; see [section 5.2](#). The purpose of the microscope was to make referent measurements which could be compared with the position measurements by the lensless sensor.

[Figure 32](#) compares the results from the sensor and the microscope. The position is calculated using a similar image-processing algorithm (see [subsection 5.3.2](#)). [Figure 32](#) confirms that despite worse image quality from the lensless sensor the position can be determined with high accuracy. Even the smallest changes are precisely measured. In comparison with the microscope, there is a higher noise in the signal

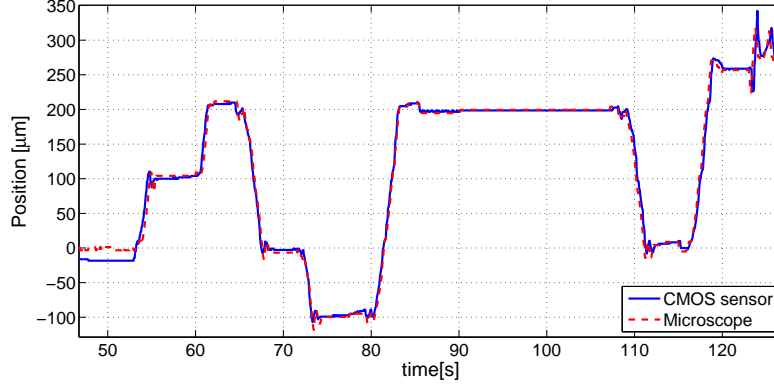


Figure 32: Position x obtained from the images captured by the lensless CMOS sensor and the microscope. The CMOS sensor was used for the feedback.

with amplitude around $2\mu\text{m}$. However, that is acceptable, because the number is small in comparison with the particle size.

5.5.2 Unit step response

To demonstrate and verify the function of the lensless sensor in the feedback loop, I measured a unit step response. The reference position was manually switched.

Due to the area the lensless sensor can cover, i.e. the real dimensions of the sensor, I chose the set of 50-micron electrodes. That allowed the control of the bead over the whole range of the electrodes. Additionally, the electrodes were easily distinguishable in the image.

To diminish the sticking I applied maximum voltage allowed by the generator, i.e. 20 V, with frequency 200 kHz. For lower voltage the bead tended to get stuck more often. Moreover, for voltage under 15 V the repelling force field was not sufficient for the bead to overcome the adjacent electrodes.

Figure 33a displays the measured response. The microbead under these conditions achieved speed approximately $300\mu\text{m s}^{-1}$; that is significantly more than on the opaque array used in [42]. The reason for that are most likely the narrower electrodes employed and thus stronger electric field. Meanwhile the error from the reference was only $3.5\mu\text{m}$.

All the responses were also recorded and are included within the files attached with the thesis. I recommend the reader to study the videos as well.

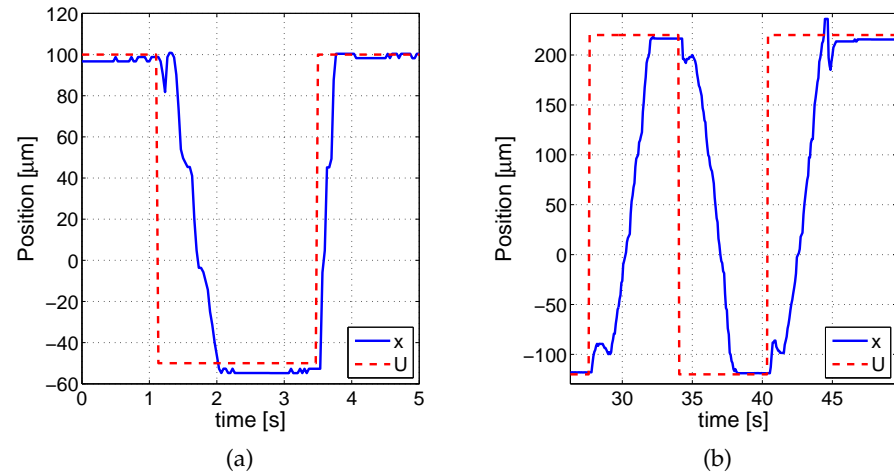


Figure 33: Recorded unit step responses. x is the detected position and U is the reference. In (a), error is around $3.5\text{ }\mu\text{m}$ while voltage was 20 V, 200 kHz. (b) shows a microbead unsticking from an electrode (18 V, 200 kHz).

5.5.3 Problems: sticking and water electrolysis

Water electrolysis

Firstly, I experienced electrolysis of the deionized water. The problem is known from the previous experiments in the laboratory. An electrode was probably damaged when too low frequency was applied; electrolysis occurs from the strong electric field.

Sticking

Sticking of the beads to the electrodes was perhaps the most significant issue that I encountered during the work on the translucent array. The degree of sticking was much higher than we have ever encountered before on any other MEA under similar conditions. The PS beads tended to stick on the electrode edges. Interestingly, that occurred only on certain electrodes.

Since the sticking occurs on the edges of the electrodes, I tried to verify whether the height of the electrodes is not the problem. Thus, the array was analysed using 3D Optical Surface Profiler (Zygo NewView 7300). The thickness was around 400 nm. Since the particle is more than a hundred times larger than the electrodes the height of the electrodes is likely not the problem. Yet, some of the electrodes appeared to have rough surface at the edges.

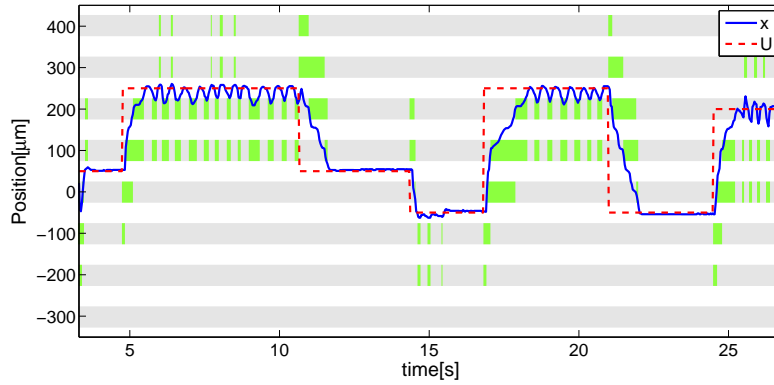


Figure 34: Sticking causes oscillation. 20 V, 200 kHz. In the background, the electrode switching sequence is showed with the regard to time (x axis). The figure displays all 8 electrodes. Green colour illustrates the on state. Notice that the electrodes above the oscillation states are almost never switched on.

Effects of sticking on control

Unfortunately, it has negative effects on the control and can be observed in the step response.

Firstly, a bead gets stuck when stopped over an electrode. [Figure 33b](#) shows the problem when the initial force is not sufficient enough to peel off a [PS](#) bead from the electrode. Notice the position response immediately after the reference change. The stack bead behaves similarly as a spring.

Further, the sticking can cause oscillations as it is illustrated in [Figure 34](#). In this case the upper edge of the electrode with distance 200 μm from the centre is problematic. When the bead achieves the position of the reference the controller turns off the adjacent electrode. Then, similarly as a spring the bead returns to the edge where it got stuck. [Figure 34](#) also displays the electrode switching sequence. Notice that the electrodes above the oscillation states are almost never turned on. It is the attractive force between the electrode and the bead which pulls the bead back.

The problem has remained unresolved. Perhaps some additional treatment of the electrodes would be helpful. Also I believe that slightly different design with smaller gaps would improve the behaviour. Finally, some papers reported improvements in sticking when a detergent dissolved in the liquid was used.

5.6 CONCLUSION

In this chapter, I verified that the lensless CMOS sensor is a full-featured alternative to the microscope in the task of position feedback

control of the 50-micron PS beads using DEP force. Obviously, other similar-sized particles responsive to the DEP would be feasible as well.

Of course, special translucent array must be used. In comparison with the opaque array employed before I observed higher degree of sticking which obstructed the control. That is discussed in [subsection 5.5.3](#). Nevertheless, this problem is probably solvable by using different method of fabrication. Also, in the future, a detergent added into the medium should be tested.

Despite that, using the feedback from the lensless sensor I was able to control the particle with precision $5\text{ }\mu\text{m}$. The maximum average speed was around $400\text{ }\mu\text{m s}^{-1}$.

For the future, I suggest using narrower gaps between the electrodes. Also, larger CMOS sensor with higher resolution could be purchased in order to cover greater area with better precision. Such sensors are abundant in today digital cameras and thus they are not so costly.

SUMMARY AND FUTURE WORK

6.1 OPTICALLY INDUCED DIELECTROPHORESIS

To sum up the foregoing, in my thesis I introduced the recent concept of **oiDEP**. **oiDEP** is an ambitious method for unrestricted planar micro-manipulation. The ultimate goal in the first part of the thesis was to reproduce the recent research successes in **oiDEP** in our conditions. I designed and built a laboratory setup for feedback control which firstly enables easy assembly and mount of the fragile **oiDEP** chip. Secondly, it allows to project high resolution light patterns on a tiny **oiDEP** chip by using two different modulation methods (**DLP** and **LC** modulator) and different light sources. And finally, it captures the image from the camera which is then processed by a specialized program I developed uniquely for this purpose. In the **oiDEP** chip I tested the viability of a new polymer material.

Before the experiments I performed various numeric simulations of the electric field within the proposed **oiDEP** chip. **PS** beads appear to be best controlled by a trap in a hollow circle. The simulation results are comparable with the behaviour reported in literature.

Although in the experiments I have not yet demonstrated the full featured manipulation in all directions, the initial tests suggest that the manipulation using the built setup for **oiDEP** is achievable. According to predictions, I observed negative dielectrophoretic force induced by the image patterns.

I tried to identify the problem which could cause the limited function. The observed movement indicates that the problem is likely either in the thickness of the used polymer layer or in the display technique. To treat that, in the future, the thickness will be increased. Also, because the polymer layer used in the **oiDEP** chip suffered from peeling, we will test a layout without the employed **PEDOT:PSS** layer.

In the future, it would be also feasible to test the spatial light modulator with other light sources (LED and laser diodes). Firstly, it would enable the incorporation of the lensless sensor in the laboratory setup as feedback for **oiDEP**. Secondly, light source with more suitable wavelength for the used polymer materials could improve the manipulation effect.

6.2 LENSLESS SENSOR

In the second part of the thesis, I verified that it is viable and convenient to use a lensless image sensor in fluidic micromanipulation.

The image lensless sensor can be used as a cheap alternative to bulky combination of a standard microscope and an off-the-shelf camera. Additionally, its use in combination with [DEP](#) or even [oiDEP](#), which I proved to be viable, can be very powerful and minimalistic combination.

When the optical path is not obstructed, the sensor is able to detect particles as small as $5\text{ }\mu\text{m}$, e.g. yeast cells or [PS](#) beads, with a LED or laser illumination due to diffraction. However, the liquid with particles must be well know; it doesn't deal well with clustering and alien particles in the optical path. Further, it would be achievable to determine the position in the third dimension using a model of scattering.

Although the cheap CMOS sensor without any optics did not offer as quality image as the microscope, once the process of manipulation is automated and sufficiently precise information can be extracted from the image, there is no such need. In the experiments, I demonstrated that the cheap lensless sensor offers the same degree of precision for automatic manipulation of 50-micron [PS](#) beads above a translucent [MEA](#).

Part I

APPENDIX

SOFTWARE

In [oiDEP](#), a computer is the essential element which links the sensor, user and the display device. Computer program acts as a controller; it generates images which are then sent to the display device. I created two separate programs: first for automatic control and second for manual control.

A.1 SOFTWARE FOR AUTOMATIC CONTROL

Image from the lensless CMOS sensor or microscope is fetched to the computer either via Firewire or via more standard USB. The task for the program is to estimate a position of the object from the image. Further, based on that information and user commands, such as a goal position of a single particle, the program should generate appropriate image patterns which are then displayed on the secondary display device.

I developed a program in Java which is capable of these tasks. There were various reasons why I chose Java over Matlab, which was used previously for particle control in [chapter 5](#). Firstly, with the given increased complexity of the parallel particle tracking and path planning, the native support of objective programming was a huge advantage. Moreover, the performance in particle recognition was poorer in Matlab and multi-threading more complicated to implement. Java could also allow envisioned extension to the mobile platform which is more suited for the user interaction

On the other hand, unlike Matlab, Java does not have many embedded tools to work with the images, which are necessary for the task. This functionality lack can be readily patched by some existing libraries. I used widely-tested Open Source Computer Vision ([OpenCV](#)) software library which extends the basic functionality by more than 2500 optimized algorithms for computer vision and machine learning. It also implements methods for easy connection of external devices such as a webcam.

Simple parallel manipulation is the main strength of the [oiDEP](#). Therefore, from the beginning I aimed for this functionality even while developing this program. Multiple particles are recognized and tracked; [GUI](#) allows user to set the target location for each particle independently and the particle is navigated there avoiding collision with other particles. Further, the average speed of each particle is measured.

This section will briefly describe all the five main parts of the program: particle recognition, particle tracking, pathfinding, pattern generation and [GUI](#).

A.1.1 *Image processing*

Image processing is composed from three steps. At first, the image is retrieved from a camera. Next, in the obtained image the objects are detected. Finally, image is displayed in [GUI](#). Before that, the program writes into the image the results of the recognition algorithm.

Various approaches could have been taken to detect the particles in the image. I was mainly restricted by the time to process the image to be able to control the objects in the real time. I had to find an algorithm which would be simple and efficient while applicable to the multiple object search. Detecting circles in the image seemed to be the most feasible solution; all objects we envision to control are of circular shape.

Circle detection is a standard task in computer vision. Methods based on Hough transform are the most widespread for this task. Although Hough transform was originally designed to detect lines, though in [\[1\]](#) it was generalized for shapes such as circles or ellipses.

[OpenCV](#) library already implements Hough circle transform.

```
void cvHoughCircles(InputArray image, OutputArray
    circles, int method, double dp, double minDist,
    double param1=100, double param2=100, int
    minRadius=0, int maxRadius=0 )
```

We can set the minimal and maximal radius of the circles. It is useful to blur the image before the processing to minimize the noise.

Image processing fetches the image, processes the image to obtain the position, and edits the image to add additional information. It runs in a separate thread independently from the particle tracking; it outputs the coordinates of the detected particles in a critical section. Likewise, from there it reads the input data such as particle information or the paths to draw it into the fetched image. Finally, the image processing displays the final edited image for the user on a monitor.

A.1.2 *Particle tracking*

Implementation of particle tracking was far from trivial.

The image is divided into square blocks with size specified by an user. The division is represented by the class `Grid`, every element of the grid (class `Cell`) can contain one particle and can be “free” or “occupied”. The grid is used later in path planning.

In the first phase, located circles by Image Processing are retrieved thirty times. Number of detections in every cell in the grid is counted

and if it exceeds 20, particle is initialized with coordinates of the cell. The class Particle contains parameters like coordinates, lives and speed.

Next, infinite cycle is started. In the first step, the program retrieves the coordinates of the detected particles (class Circle) stored in the critical section. Class Circle contains x and y coordinates, as well as the radius of the detected object. Secondly, for every particle in the memory the nearest detected circle is used to update the current coordinates. However, one detected circle is used only once. Then, particle is killed if there was not a detection in the adjacent area. Every particle begins with 100 lives; when the number of lives plunges to zero the particle is deleted. Finally, current locations of the particles to be displayed in GUI are saved into the critical section so it can be used by the thread for Image Processing.

I finally did not add the functionality to detect new particles while the program is running; it did not seem to be useful at the moment. User can reset the tracking to achieve a similar result.

Average speed of particle is measured and displayed in GUI. Every particle have implementation of the class ParticleMeasureSpeed which provides this functionality. Due to the noise, particle speed would be inaccurate. Assuming that the noise is white and thus uniformly distributed; more accurate position of the particle is obtained by averaging the position from last 60 frames. Then, positions are buffered for 10 seconds and from that the position change and average speed is obtained.

Figure 35 visualizes the function of Image Processing and Particle Tracking.

A.1.3 Pathfinding

Other crucial part of the program is the path planning. For each object, the user can set the target location where the particle should be transported to. Particle, however, cannot travel over straight trajectories as there are obstacles. At the moment I assumed only other circular particles obstruct the way in the area of interest. Nevertheless, more general solution could be sought later.

The problem is simple in case that the user would want to manipulate only with one object at a time. For instance, popular algorithm A* can be readily used for that. A* isn't the only possible solution; there is number of different algorithms fit for the problem.

However, as it was mentioned, independent parallel manipulation is highly desirable. That, of course, leads to much more complicated problem of multi-agent path planning.

Multi-agent path planning has been studied with motivation in motion planning in robotics, air traffic control or computer games, to mention a few applications. [34] suggests extensions to A* to en-

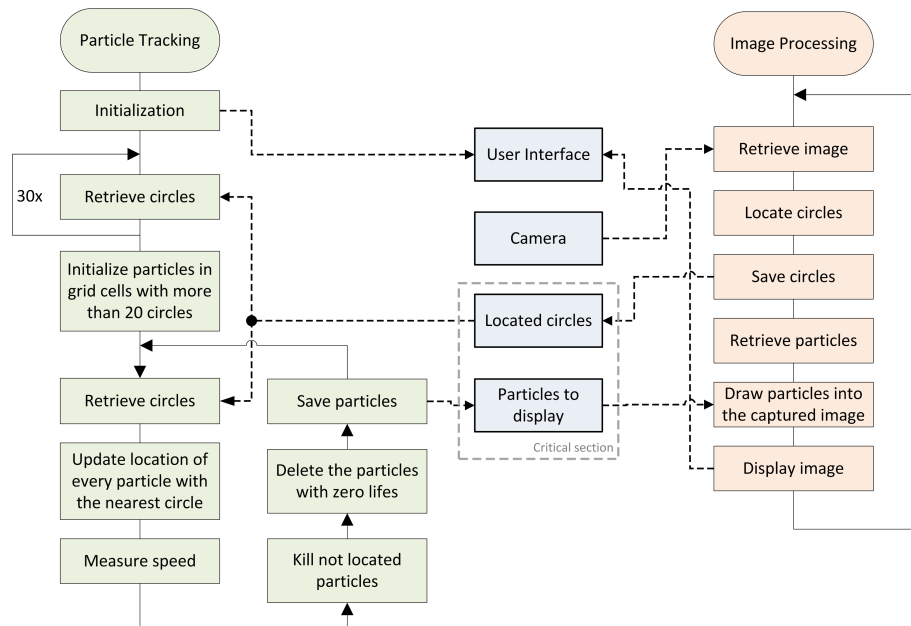


Figure 35: Simplified flow chart which illustrates the function of the program, namely the particle tracking and image processing function. Particle Tracking and Image Processing runs in separate threads.

compass the multiple agents: **LRA***, Hierarchical Cooperative A* and windowed hierarchical cooperative A* (**WHCA***). From these, **WHCA*** proved in [34] to be the most successful for vast state space and big number of agents. It also deals well with deadlocks and cycles unlike the **LRA***. Additionally, **WHCA*** allows cooperation between agents after they reached their target location. That is, when for example narrow passage is blocked by an agent this agent will cooperate and get out of the way.

Nevertheless, **LRA*** is still widespread and actually sufficient for this application as the environment is far from difficult. **WHCA*** could be implemented in the future if there will be the reason for that. In **LRA***, each agent searches for the optimal path ignoring other agents except the adjacent ones. When the path is blocked, the path is recalculated with the possibility to wait 2 steps. Indeed, deadlocks and cycles are possible. However, they don't pose such a problem in this application.

A.1.4 Virtual electrodes generation

If the feedback control is turned on, the program display control patterns in a separate window based on the generated paths by path planning (Class FeedbackCanvas). The problem is that the projection is never exactly aligned with the area of manipulation, i.e. the position of the sensor. To correct that, we should allow the user to

calibrate the position of the image; through the GUI he can change the vertical and horizontal position, rotation, and the scale of the objects. In the future, this could be done automatically from the image feedback.

A.1.5 *Graphical user interface*

GUI of the program for automatic control has three basic functions:

- it displays the postprocessed image from the camera and output from the algorithm like speed of the moving particle,
- it allows user to capture the image from the camera,
- it also enables him to change the settings for control and image recognition,
- and finally to set an arbitrary position as the goal location for the detected objects by clicking directly on the capture image.

The image of the GUI is placed in the main text on page 37.

A.1.6 *Conclusion and performance*

In theory, the program should allow automatic manipulation. Unfortunately, the individual parts could have been tested only separately. I could verify that the image recognition in the image from the lensless sensor is quite robust despite high noise. Its performance was around 10 fps. An example of the processed image is in Figure 12b on page 25. I have not yet demonstrated the feedback because the CMOS sensor wasn't compatible with the display techniques. That is discussed in chapter 4. While for the microprojector, the image blinked; for the laser light modulator, the image for impaired by diffraction. However different projection methods will solve that. All this should be finished in the future.

A.2 SOFTWARE FOR MANUAL CONTROL

The main purpose of the program for manual control was to simplify the initial testing of the oiDEP concept. I sought maximum variability and intuitiveness for the user.

The program resembles a simple graphical editor. There are two frames. User can load and add arbitrary image shapes in 32bit PNG format to the canvas in the first frame (CTRL+L or button in the panel). The image objects are draggable (using mouse or keyboard arrows after selection of the object) and resizable (CTRL+scroll). Therefore, more complicated shapes can be easily built and quickly altered.

The input images should have black foreground while the background is transparent. Foreground and background colour can be then quickly modified from the panel. That proved to be a convenient feature.

Additionally, for every object user have the option to load an alternative image by pressing CTRL+L while the object is selected. Then button “A” switches between the alternative and original image. That allows swift change of the objects. For instance simple crane can be created.

The changes in the first frame for user control are immediately mirrored to the second frame. Only, the object size is proportionally adjusted. This frame runs in a fullscreen mode on the modulator which is treated as a second display by the operating system. The window setup allows the user to control the particle position while running other tasks on the same monitor, e.g. observing the image from a camera.

Finally, basic functions are implemented. The user can save the current session and load the previous sessions. Standard shortcuts can be used (CTRL+S, CTRL+O, Delete).

I prepared simple shapes which allow the particle trapping based on the simulations from [chapter 2](#) and shapes used in literature. The program was used for initial experiments with different photosensitive layers discussed in [section 4.5](#).

INDEPENDENT CONTROL OF MULTIPLE OBJECTS ON AN INTERDIGITATED ARRAY

Together with Jiří Zemánek, we proposed an algorithm for an independent control of multiple objects with a simple interdigitated array. The algorithm is devised for two objects at the moment but the idea is scalable. Obviously, this task is straightforward while the particles are far apart because the dependence is minimal. However, since the DEP force acting on the particles aligned along the electrodes is (almost) the same we are restricted. Thus, the ability to interchange them is crucial for the function.

B.1 THE ALGORITHM FOR OBJECT INTERCHANGING

For that we utilize the fact that the field slightly differs along the electrodes. Besides that, each particle slightly differs from the others. We oscillate with the particles above a location where we can create an unstable equilibrium. When the particles reach this position the algorithm switches to a state with the unstable equilibrium. Three outcomes are now possible:

- both objects fall on the same side of the electrode,
- objects are separated but they are not interchanged,
- objects are interchanged.

Besides the latter case, we repeat the procedure from the start. This is repeated until the particles are interchanged. The algorithm is in fact a state automaton; see [Figure 36a](#). This iterative method allows to find the unknown equilibrium position by adjusting a special parameter b according to the outcome of the separation. The method can be further refined by using two triggers b_{up} and b_{down} for both direction separately.

On the interdigitated translucent array such position can be found in the middle of three electrodes. The two peripheral electrodes serve for the oscillation and the middle electrode switches on the unstable equilibrium; see [Figure 36b](#).

B.2 EXPERIMENTS AND DISCUSSION

Unfortunately, the sticking greatly aggravated the experiments. In the experiments I was able to carry out maximally seven tests in a row with the same two beads because after a while one of the beads

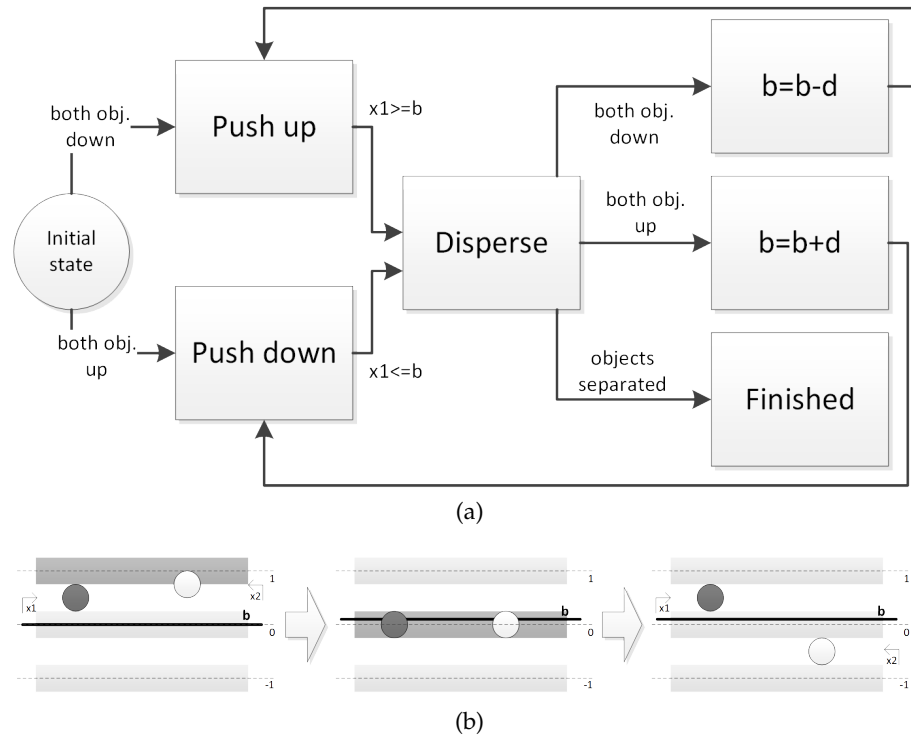


Figure 36: Principle of multiple object separation on a simple parallel array. (a) describes the heart of the algorithm. It is a state automaton with two inputs: positions $x1$ and $x2$ as depicted in (b), the output is a control action (vector of binary values setting an electrodes on or off). Meanwhile (b) illustrates the steps of the automation. The darker color highlights a switched-on electrode. b is a variable parameter which triggers the control action creating the unstable equilibrium.

got stuck. The sticking is described in [Section 5.5.3](#). Even though the results are promising.

The included video captures one of the experiments. The experimental setup was the same as in the [Section 5.2](#) except I observed the array with a microscope. The reason for that was only a convenience. The algorithm ran for seven times with the same beads and almost same initial conditions. Four times out of seven the leftmost bead fell into the lower region. This trend was typical.

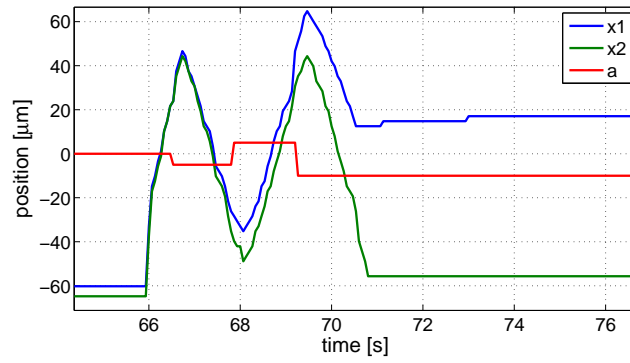


Figure 37: Typical position sequence during the separation of multiple objects. x_1 and x_2 are the positions of the particles on the left and on the right respectively. d is the position of the trigger which iteratively adjusts. Notice that it is different for up and down direction.

CD CONTENTS

- Videos from experiments from [Section 4.5](#), [Section 5.5](#) and from [Appendix B](#).
- Videos from simulations from [Section 2.6](#).
- Source codes and documentation of the program for automatic control for the [oiDEP](#) described in [Section A.1](#).
- Source codes and documentation of the program for manual control for the [oiDEP](#) device described in [Section A.2](#).
- Feedback controller from [Chapter 5](#) implemented in Simulink.
- a Matlab package MatScat for simulating scattering of electromagnetic radiation by a sphere based on Mie Theory Schäfer [\[33\]](#).
- Electronic version of the thesis in PDF.

BIBLIOGRAPHY

- [1] D. H. Ballard. Generalizing the hough transform to detect arbitrary shapes. *Pattern recognition*, 13(2):111–122, 1981. URL <http://www.sciencedirect.com/science/article/pii/0031320381900091>. (Cited on page 58.)
- [2] C. F. Bohren and D. R. Huffman. *Absorption and scattering of light by small particles*. Wiley-Vch, 2008. URL http://www.google.com/books?hl=en&lr=&id=ib3EMXXIRXUC&oi=fnd&pg=PP2&dq=bohren&ots=Axhovcad2Q&sig=b1kEKv071Vln-g75-0Q479_9H7I. (Cited on pages 27, 28, and 29.)
- [3] S. Childress. *An Introduction to Theoretical Fluid Mechanics*. American Mathematical Soc. ISBN 9780821883587. (Cited on pages 15 and 17.)
- [4] P.-Y. Chiou. *Massively parallel optical manipulation of single cells, micro-and nano-particles on optoelectronic devices*. PhD thesis, UNIVERSITY OF CALIFORNIA, 2005. URL <http://www.eecs.berkeley.edu/Pubs/Dissertations/Data/8294.pdf>. (Cited on pages 9 and 10.)
- [5] P.-Y. Chiou, Z. Chang, and M. Wu. A novel optoelectronic tweezer using light induced dielectrophoresis. In *2003 IEEE/LEOS International Conference on Optical MEMS*, pages 8–9, 2003. doi: 10.1109/OMEMS.2003.1233441. (Cited on page 9.)
- [6] P.-Y. Chiou, W. Wong, J. Liao, and M. Wu. Cell addressing and trapping using novel optoelectronic tweezers. In *Micro Electro Mechanical Systems, 2004. 17th IEEE International Conference on. (MEMS)*, pages 21 – 24, 2004. doi: 10.1109/MEMS.2004.1290512. (Cited on page 9.)
- [7] P.-Y. Chiou, A. Ohta, and M. Wu. Microvision-activated automatic optical manipulator for microscopic particles [microvision read microvision]. In *18th IEEE International Conference on Micro Electro Mechanical Systems, 2005. MEMS 2005*, pages 682–685, 2005. doi: 10.1109/MEMS.2005.1454021. (Cited on page 1.)
- [8] P.-Y. Chiou, A. T. Ohta, and M. C. Wu. Massively parallel manipulation of single cells and microparticles using optical images. *Nature*, 436(7049):370–372, 2005. URL <http://www.nature.com/nature/journal/v436/n7049/abs/nature03831.html>. (Cited on page 11.)

- [9] W. Choi, S.-W. Nam, H. Hwang, S. Park, and J.-K. Park. Programmable manipulation of motile cells in optoelectronic tweezers using a grayscale image. *Applied Physics Letters*, 93(14): 143901–143901–3, 2008. ISSN 0003-6951. doi: 10.1063/1.2996277. (Cited on page 9.)
- [10] P. K. Dasgupta and S. Liu. Electroosmosis: a reliable fluid propulsion system for flow injection analysis. *Analytical Chemistry*, 66(11):1792–1798, 1994. URL <http://pubs.acs.org/doi/pdf/10.1021/ac00083a004>. (Cited on page 8.)
- [11] N. G. Green, A. Ramos, A. González, H. Morgan, and A. Castellanos. Fluid flow induced by nonuniform ac electric fields in electrolytes on microelectrodes. i. experimental measurements. *Physical Review E*, 61(4):4011–4018, Apr. 2000. doi: 10.1103/PhysRevE.61.4011. URL <http://link.aps.org/doi/10.1103/PhysRevE.61.4011>. (Cited on pages 8 and 18.)
- [12] D. J. Harrison, A. Manz, Z. Fan, H. Luedi, and H. M. Widmer. Capillary electrophoresis and sample injection systems integrated on a planar glass chip. *Analytical chemistry*, 64(17): 1926–1932, 1992. URL <http://pubs.acs.org/doi/abs/10.1021/ac00041a030>. (Cited on page 8.)
- [13] P. J. Hesketh, M. A. Gallivan, S. Kumar, C. J. Erdy, and Z. L. Wang. The application of dielectrophoresis to nanowire sorting and assembly for sensors. In *Intelligent Control, 2005. Proceedings of the 2005 IEEE International Symposium on, Mediterrean Conference on Control and Automation*, page 153–158, 2005. URL http://ieeexplore.ieee.org/xpls/abs_all.jsp?arnumber=1467007. (Cited on page 1.)
- [14] Y. Higuchi, T. Kusakabe, T. Tanemura, K. Sugano, T. Tsuchiya, and O. Tabata. Manipulation system for nano/micro components integration via transportation and self-assembly. In *IEEE 21st International Conference on Micro Electro Mechanical Systems, 2008. MEMS 2008*, pages 836 –839, Jan. 2008. doi: 10.1109/MEMSYS.2008.4443786. (Cited on page 10.)
- [15] H.-y. Hsu, A. T. Ohta, P.-Y. Chiou, A. Jamshidi, S. L. Neale, and M. C. Wu. Phototransistor-based optoelectronic tweezers for dynamic cell manipulation in cell culture media. *Lab on a Chip*, 10(2):165–172, Dec. 2009. ISSN 1473-0189. doi: 10.1039/B906593H. URL <http://pubs.rsc.org/en/content/articlelanding/2010/lc/b906593h>. (Cited on page 9.)
- [16] C. Huang, J. Zhu, L. Wang, M. Guo, J. Yu, and J. Cheng. Automated dielectrophoretic cell fractionation system using MEMS

- technology. In *1st IEEE International Conference on Nano/Micro Engineered and Molecular Systems*, 2006. NEMS '06, pages 1422–1427, 2006. doi: 10.1109/NEMS.2006.334780. (Cited on page 1.)
- [17] Y. Huang, J. Yang, X.-B. Wang, F. F. Becker, and P. R. Gascoyne. The removal of human breast cancer cells from hematopoietic CD34 + stem cells by dielectrophoretic field-flow-fractionation. *Journal of Hematotherapy & Stem Cell Research*, 8(5):481–490, Oct. 1999. ISSN 1525-8165. doi: 10.1089/152581699319939. URL <http://online.liebertpub.com/doi/abs/10.1089/152581699319939>. (Cited on pages 1 and 7.)
- [18] M. P. Hughes. *Nanoelectromechanics in engineering and biology*. CRC press, 5 edition, 2010. (Cited on page 16.)
- [19] H. Hwang, Y.-J. Choi, W. Choi, S.-H. Kim, J. Jang, and J.-K. Park. Interactive manipulation of blood cells using a lens-integrated liquid crystal display based optoelectronic tweezers system. *Electrophoresis*, 29(6):1203–1212, Mar. 2008. ISSN 0173-0835. doi: 10.1002/elps.200700415. PMID: 18297658. (Cited on pages 9 and 32.)
- [20] A. Jamshidi, P. J. Pauzauskie, P. J. Schuck, A. T. Ohta, P.-Y. Chiou, J. Chou, P. Yang, and M. C. Wu. Dynamic manipulation and separation of individual semiconducting and metallic nanowires. *Nature photonics*, 2(2):86–89, 2008. URL <http://www.nature.com/nphoton/journal/v2/n2/abs/nphoton.2007.277.html>. (Cited on page 9.)
- [21] X. Ma, J. Q. Lu, R. S. Brock, K. M. Jacobs, P. Yang, and X.-H. Hu. Determination of complex refractive index of polystyrene microspheres from 370 to 1610 nm. *Physics in medicine and biology*, 48(24):4165, 2003. URL <http://iopscience.iop.org/0031-9155/48/24/013>. (Cited on page 29.)
- [22] Z. Ma, H. G. Merkus, J. G. de Smet, C. Heffels, and B. Scarlett. New developments in particle characterization by laser diffraction: size and shape. *Powder Technology*, 111(1–2):66–78, Aug. 2000. ISSN 0032-5910. doi: 10.1016/S0032-5910(00)00242-4. URL <http://www.sciencedirect.com/science/article/pii/S0032591000002424>. (Cited on page 27.)
- [23] Y. Majima, K. Yamagata, and M. Iwamoto. Spatial charge distribution of organic-molecular-beam-deposited titanylphthalocyanine on metal electrodes. In *Proceedings of 1998 International Symposium on Electrical Insulating Materials*, 1998, pages 527–530, 1998. doi: 10.1109/ISEIM.1998.741797. (Cited on page 18.)
- [24] G. H. Markx, M. S. Talary, and R. Pethig. Separation of viable and non-viable yeast using dielectrophoresis. *Journal of*

- Biotechnology*, 32(1):29–37, 1994. ISSN 0168-1656. doi: 10.1016/0168-1656(94)90117-1. URL <http://www.sciencedirect.com/science/article/pii/0168165694901171>. (Cited on page 1.)
- [25] H. Morgan and N. G. Green. *AC electrokinetics: colloids and nanoparticles*. Number 2. Research Studies Press, 2003. URL <http://eprints.gla.ac.uk/33024/>. (Cited on pages 6, 7, and 9.)
- [26] A. Ohta, P.-Y. Chiou, T. Han, J. Liao, U. Bhardwaj, E. McCabe, F. Yu, R. Sun, and M. Wu. Dynamic cell and microparticle control via optoelectronic tweezers. *Journal of Microelectromechanical Systems*, 16(3):491–499, 2007. ISSN 1057-7157. doi: 10.1109/JMEMS.2007.896717. (Cited on pages 1 and 9.)
- [27] B. Ovryn. Three-dimensional forward scattering particle image velocimetry applied to a microscopic field-of-view. *Experiments in fluids*, 29(1):S175–S184, 2000. URL <http://link.springer.com/article/10.1007/s003480070019>. (Cited on pages 27 and 29.)
- [28] R. Pethig. Review Article—Dielectrophoresis: status of the theory, technology, and applications. *Biomicrofluidics*, 4(2):022811–022811–35, June 2010. doi: doi:10.1063/1.3456626. URL http://bmf.aip.org/resource/1/biomgb/v4/i2/p022811_s1?isAuthorized=no. (Cited on page 1.)
- [29] R. Pethig. Review article—dielectrophoresis: Status of the theory, technology, and applications. *Biomicrofluidics*, 4(2), June 2010. ISSN 1932-1058. doi: 10.1063/1.3456626. URL <http://www.ncbi.nlm.nih.gov/pmc/articles/PMC2917862/>. PMID: 20697589 PMCID: PMC2917862. (Cited on page 6.)
- [30] H. A. Pohl. *Dielectrophoresis: the behavior of neutral matter in nonuniform electric fields*, volume 80. Cambridge university press Cambridge, 1978. URL <http://www.getcited.org/pub/101783535>. (Cited on page 5.)
- [31] H. A. Pohl and I. Hawk. Separation of living and dead cells by dielectrophoresis. *Science*, 152(3722):647–649, 1966. URL <http://www.sciencemag.org/content/152/3722/647.1.short>. (Cited on pages 1 and 7.)
- [32] A. Ramos, H. Morgan, N. G. Green, and A. Castellanos. AC electric-field-induced fluid flow in microelectrodes. *Journal of Colloid and Interface Science*, 217(2):420–422, Sept. 1999. ISSN 0021-9797. doi: 10.1006/jcis.1999.6346. URL <http://www.sciencedirect.com/science/article/pii/S0021979799963464>. (Cited on page 8.)

- [33] J.-P. Schäfer. *Implementierung und Anwendung analytischer und numerischer Verfahren zur Lösung der Maxwellgleichungen für die Untersuchung der Lichtausbreitung in biologischem Gewebe*. PhD thesis, Ph. D. thesis, 2011. URL <http://d-nb.info/1016659563/34>. (Cited on pages 29 and 67.)
- [34] D. Silver. Cooperative pathfinding. In *The 1st Conference on Artificial Intelligence and Interactive Digital Entertainment (AIIDE'05)*, page 23–28, 2005. URL <http://www.aaai.org/Papers/AIIDE/2005/AIIDE05-020.pdf>. (Cited on pages 59 and 60.)
- [35] H. Tada, H. Touda, M. Takada, and K. Matsushige. Quasi-intrinsic semiconducting state of titanyl-phthalocyanine films obtained under ultrahigh vacuum conditions. *Applied Physics Letters*, 76(7):873–875, 2000. URL http://ieeexplore.ieee.org/xpls/abs_all.jsp?arnumber=4904197. (Cited on page 18.)
- [36] J. K. Valley, A. Jamshidi, A. T. Ohta, H.-Y. Hsu, and M. C. Wu. Operational regimes and physics present in optoelectronic tweezers. *Journal of microelectromechanical systems : a joint IEEE and ASME publication on microstructures, microactuators, microsensors, and microsystems*, 17(2):342–350, Apr. 2008. ISSN 1057-7157. doi: 10.1109/JMEMS.2008.916335. URL <http://www.ncbi.nlm.nih.gov/pmc/articles/PMC2600567/>. PMID: 19079767 PMCID: PMC2600567. (Cited on page 17.)
- [37] K. Visser. Electric conductivity of stationary and flowing human blood at low frequencies. In *Engineering in Medicine and Biology Society, 1989. Images of the Twenty-First Century., Proceedings of the Annual International Conference of the IEEE Engineering in*, pages 1540–1542 vol.5, 1989. doi: 10.1109/IEMBS.1989.96329. (Cited on page 9.)
- [38] W. Wang, Y.-H. Lin, R.-S. Guan, T.-C. Wen, T.-F. Guo, and G.-B. Lee. Bulk-heterojunction polymers in optically-induced dielectrophoretic devices for the manipulation of microparticles. *Optics Express*, 17(20):17603–17613, 2009. doi: 10.1364/OE.17.017603. URL <http://www.opticsexpress.org/abstract.cfm?URI=oe-17-20-17603>. (Cited on pages 10 and 13.)
- [39] S.-M. Yang, T.-M. Yu, H.-P. Huang, M.-Y. Ku, S.-Y. Tseng, C.-L. Tsai, H.-P. Chen, L. Hsu, and C.-H. Liu. Light-driven manipulation of picobubbles on a titanium oxide phthalocyanine-based optoelectronic chip. *Applied Physics Letters*, 98(15):153512–153512–3, Apr. 2011. ISSN 00036951. doi: doi:10.1063/1.3580760. URL http://apl.aip.org/resource/1/applab/v98/i15/p153512_s1?bypassSS0=1. (Cited on page 10.)
- [40] T.-M. Yu, S.-M. Yang, H.-P. Huang, M.-Y. Ku, S.-Y. Tseng, M.-H. Liu, L. Hsu, and C.-H. Liu. Organic photoconductive dielec-

- trophoresis by using titanium oxide phthalocyanine for micro-particles manipulation. In *Micro Electro Mechanical Systems (MEMS), 2010 IEEE 23rd International Conference on*, pages 1119–1122, Jan. 2010. doi: 10.1109/MEMSYS.2010.5442407. (Cited on pages 10 and 12.)
- [41] J. Zemánek. *Noncontact parallel manipulation with micro- and mesoscale objects using dielectrophoresis*. Czech Technical University in Prague, Prague, Czech Republic, 2009. (Cited on page 1.)
- [42] J. Zemánek and Z. Hurák. Visual feedback position control for negative dielectrophoresis. *sent for review*, 2013, 2013. (Cited on pages 43, 48, and 49.)
- [43] J. Zemánek, Z. Hurák, and Y. Bellouard. Modeling and simulation, design and fabrication, instrumentation and control for dielectrophoresis. In *25th International Symposium on Microscale BioSeparations MSB 2010*, volume 1, page 118, Prague, Czech Republic, Mar. 2010. Ústav analytické chemie AV ČR, v. v. i. ISBN ISBN 978-80-254-6631-5. URL <http://www.genomac.cz/msb2010>. (Cited on page 1.)
- [44] J. Zemánek, Z. Hurák, and Y. Bellouard. Corner microelectrode array for planar dielectrophoretic manipulation. *sent for review*, 2013. (Cited on page 1.)